

Assessing recent trends in high-latitude Southern Hemisphere surface climate

Julie M. Jones^{1*}, Sarah T. Gille², Hugues Goosse³, Nerilie J. Abram⁴, Pablo O. Canziani⁵, Dan J. Charman⁶, Kyle R. Clem⁷, Xavier Crosta⁸, Casimir de Lavergne⁹, Ian Eisenman², Matthew H. England¹⁰, Ryan L. Fogt¹¹, Leela M. Frankcombe¹⁰, Gareth J. Marshall¹², Valérie Masson-Delmotte¹³, Adele K. Morrison¹⁴, Anaïs J. Orsi¹³, Marilyn N. Raphael¹⁵, James A. Renwick⁷, David P. Schneider¹⁶, Graham R. Simpkins¹⁷, Eric J. Steig¹⁸, Barbara Stenni¹⁹, Didier Swingedouw⁸ and Tessa R. Vance²⁰.

Understanding the causes of recent climatic trends and variability in the high-latitude Southern Hemisphere is hampered by a short instrumental record. Here, we analyse recent atmosphere, surface ocean and sea-ice observations in this region and assess their trends in the context of palaeoclimate records and climate model simulations. Over the 36-year satellite era, significant linear trends in annual mean sea-ice extent, surface temperature and sea-level pressure are superimposed on large interannual to decadal variability. Most observed trends, however, are not unusual when compared with Antarctic palaeoclimate records of the past two centuries. With the exception of the positive trend in the Southern Annular Mode, climate model simulations that include anthropogenic forcing are not compatible with the observed trends. This suggests that natural variability overwhelms the forced response in the observations, but the models may not fully represent this natural variability or may overestimate the magnitude of the forced response.

The high-latitude Southern Hemisphere (SH) is a highly complex and critically important component of the global climate system that remains poorly understood. The Antarctic Ice Sheet represents the greatest potential source of global sea-level rise¹, and its response to climate change is a key source of uncertainty for future projections^{2,3}. The Southern Ocean is important for its ability to take up heat and carbon dioxide, and thereby mitigate human-induced atmospheric temperature and CO₂ rise^{4–8}. Antarctic sea ice is important for its role in ocean–atmosphere exchange and provides an important climate feedback through its influence on albedo and atmospheric and oceanic circulation.

The leading mode of atmospheric circulation variability in the SH high latitudes is the Southern Annular Mode (SAM)⁹. It is a measure of the mid-to-high-latitude atmospheric pressure gradient and reflects the strength and position of the westerly winds that circle Antarctica. This in turn affects various aspects of Antarctic

climate and controls the timing and distribution of rainfall received by the mid-latitude SH continents¹⁰. An almost equally important aspect of large-scale circulation variability in this region is the mid-to-high-latitude response to tropical variability, particularly the El Niño/Southern Oscillation (ENSO)¹¹.

Over recent decades, multiple changes have been observed in high-latitude SH climate. But the brevity and sparse distribution of observational records pose considerable challenges to understanding whether observed changes are anthropogenically forced or remain within the range of natural climate variability. We can improve our understanding of SH high-latitude climate by combining information from instrumental, satellite, palaeoclimate and reanalysis data, along with climate model simulations. Here, we provide an assessment of recent changes in the atmosphere, ocean and sea-ice systems of the southern high latitudes (south of 50° S), on timescales from decades to centuries. We describe SH climate trends using

¹Department of Geography, University of Sheffield, Sheffield S10 2TN, UK. ²Scripps Institution of Oceanography, University of California San Diego, La Jolla, California 92093, USA. ³ELIC/TECLIM Université catholique de Louvain, Place Pasteur 3, 1348 Louvain-la-Neuve, Belgium. ⁴Research School of Earth Sciences and ARC Centre of Excellence for Climate System Science, The Australian National University, Canberra ACT 2601, Australia. ⁵Unidad de Investigación y Desarrollo de las Ingenierías, Facultad Regional Buenos Aires, Universidad Tecnológica Nacional/CONICET, Argentina. ⁶Department of Geography, College of Life and Environmental Sciences, University of Exeter, EX4 1RJ, UK. ⁷School of Geography, Environment, and Earth Sciences, Victoria University of Wellington, Wellington 6012, New Zealand. ⁸Environnements et Paléoenvironnements Océaniques et Continentaux (UMR EPOC 5805), University of Bordeaux, Allée Geoffroy St Hilaire, 33615 Pessac, France. ⁹Sorbonne Universités (Université Pierre et Marie Curie Paris 6)-CNRS-IRD-MNHN, LOCEAN Laboratory, F-75005 Paris, France. ¹⁰ARC Centre of Excellence for Climate System Science, The University of New South Wales, Sydney, New South Wales 2052, Australia. ¹¹Department of Geography, Ohio University, Athens, Ohio 45701, USA. ¹²British Antarctic Survey, High Cross, Madingley Road, Cambridge CB3 0ET, UK. ¹³Laboratoire des Sciences du Climat et de l'Environnement, LSCE/IPSL, CEA-CNRS-UVSQ, Université Paris-Saclay, France. ¹⁴Program in Atmospheric and Oceanic Sciences, Princeton University, 300 Forrester Rd, Princeton, New Jersey 08544, USA. ¹⁵Department of Geography, University of California Los Angeles, 1255 Bunche Hall, Los Angeles, California 90095, USA. ¹⁶National Center for Atmospheric Research, PO Box 3000, Boulder, Colorado 80307-3000, USA. ¹⁷Department of Earth System Science, University of California, Irvine, Croul Hall, Irvine, California 92697-3100, USA. ¹⁸Department of Earth and Space Sciences, University of Washington, 70 Johnson Hall, Box 351310, Seattle, Washington 98195, USA. ¹⁹Department of Environmental Sciences, Informatics and Statistics, Ca' Foscari University of Venice, Italy, Via Torino 155, 30170 Venezia Mestre, Italy. ²⁰Antarctic Climate and Ecosystems Cooperative Research Centre, Private Bag 80, Hobart, Tasmania 7001, Australia. *e-mail: julie.jones@sheffield.ac.uk

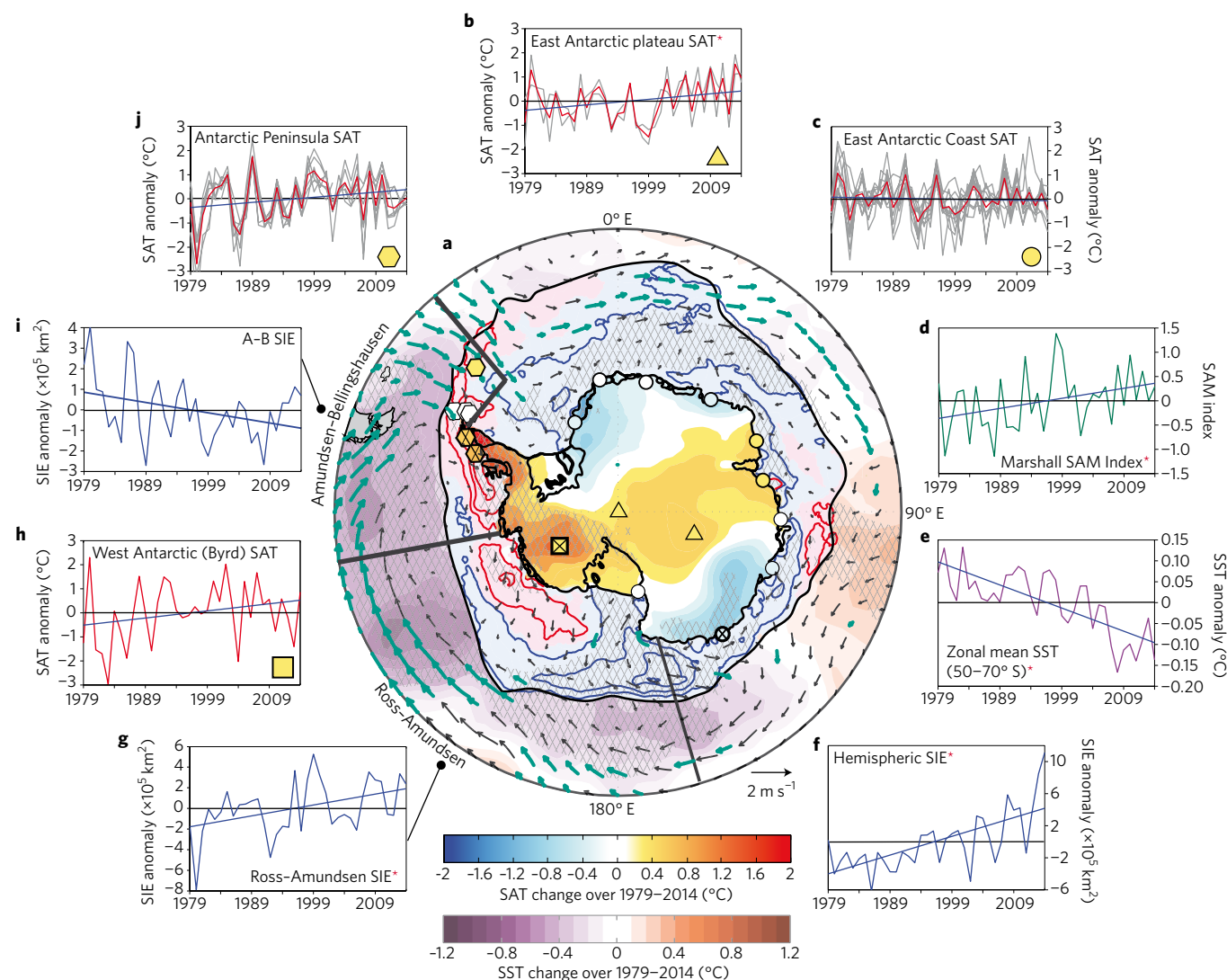


Figure 1 | Antarctic atmosphere-ocean-ice changes over the satellite-observing era. **a**, Total changes over 1979–2014 in annual mean surface air temperature (blue-red shading), station-based surface air temperature (SAT, blue-red shaded shapes), sea-ice concentration (contours, 10% intervals; red and blue contours, alongside light pink and blue shading beneath, denote negative and positive trends, respectively), sea surface temperature (SST, purple-red shading), and 10-m winds (vectors). Only SST trends equatorward of the climatological September sea-ice extent (SIE, black contour) are shown. Hatching and teal vectors highlight trends significant at the 95% level according to two-tailed Student’s *t*-tests. Note that SAT trends are calculated over 1979–2012 but scaled to represent trends over the 36-year period 1979–2014. **b–j**, Surrounding figures show time-series: East Antarctic plateau SAT (**b**; triangles; red line denotes multi-station mean, grey lines those of individual East Antarctic plateau stations); East Antarctic coast SAT (**c**; circles; red line denotes multi-station mean, grey lines those of individual East Antarctic coast stations); the Marshall Southern Annular Mode index (**d**; difference in station sea-level pressure between 40° and 65° S); Southern Ocean zonal mean SST (**e**; averaged over 50–70° S); Southern Hemisphere SIE (**f**); Ross-Amundsen SIE (**g**); West Antarctic SAT (**h**; square; Byrd Station); Amundsen-Bellinghousen SIE (**i**); and Antarctic Peninsula SAT (**j**; hexagons; red line denotes multi-station mean, grey lines those of individual Antarctic Peninsula stations). For all time series, blue lines highlight the linear trend, and red asterisks where the trend is significant at the 95% level according to a two-tailed Student’s *t*-test. See Supplementary Methods for details on datasets and trend significance calculation.

satellite information (1979–2014) and Antarctic station observations. These are compared with trends and multi-decadal variability from palaeoclimate data spanning the past 200 years, as well as control and forced climate simulations from the Fifth Climate Model Intercomparison Project (CMIP5)¹², to assess whether recent trends are unusual compared with natural variability. We conclude by identifying key knowledge gaps where strategically focused research will improve understanding of the contribution of SH high latitudes to global climate variability and change.

Antarctic climate monitoring

Coordinated international efforts to monitor Antarctic climate

began in the International Geophysical Year of 1957/58. Few climate measurements are available, however, over vast areas of the continent and the adjacent ice-shelves, sea ice and oceans. The advent of routine satellite sounder observations in 1979 revolutionized knowledge of climate over Antarctica and the surrounding oceans, although uncertainties remain, owing to satellite sensor changes¹³. More uncertain early satellite estimates of sea ice extend back to 1972 (ref. 14), with ongoing recovery of ice edge information for the 1964–1972 period^{15,16}. Knowledge of recent subsurface ocean trends remains more limited. The Argo profiling float programme and conductivity–temperature–depth tags mounted on elephant seals have provided substantial numbers of subsurface

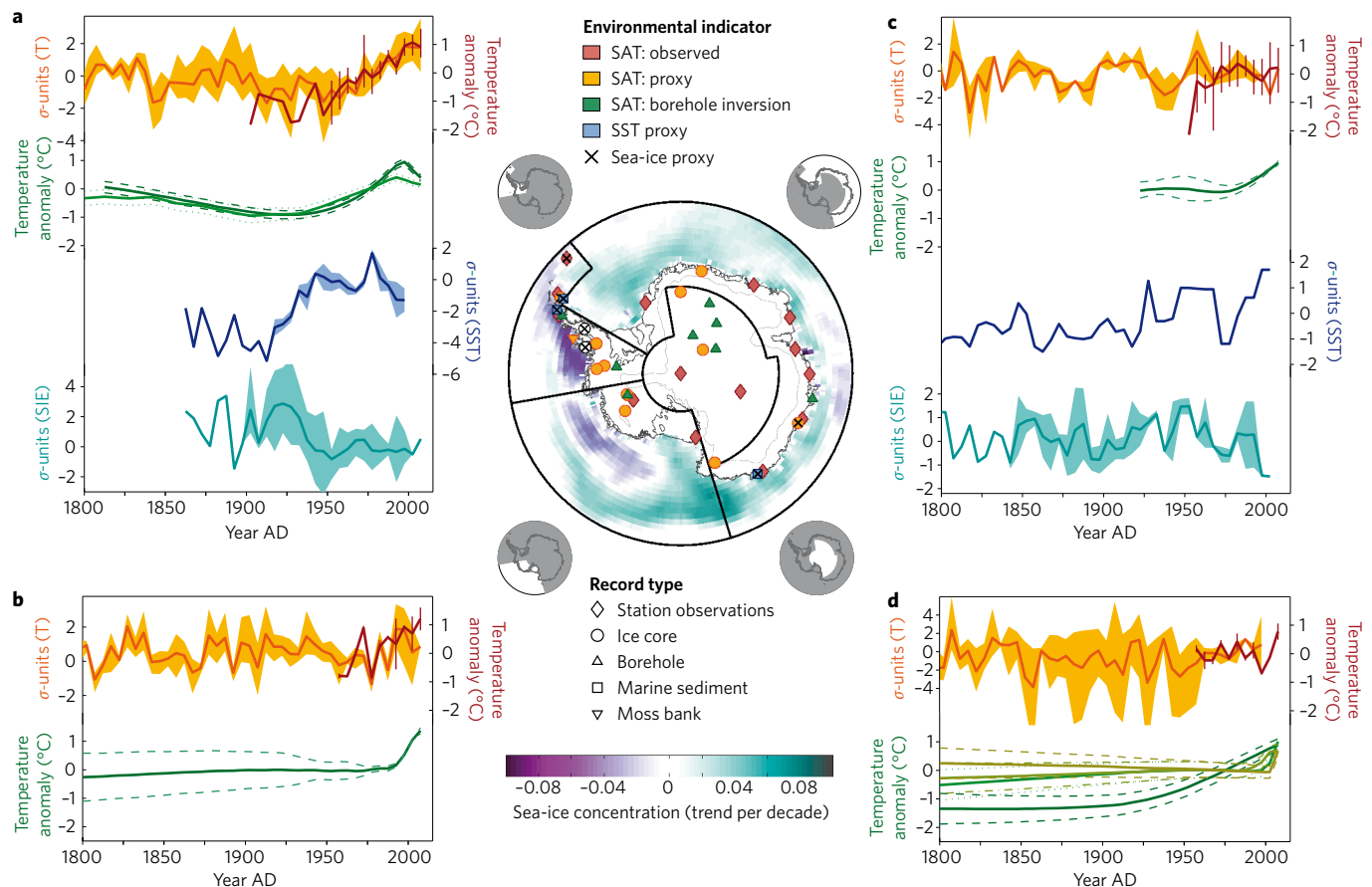


Figure 2 | Antarctic climate variability and trends over the past 200 years from long observational and proxy-derived indicators. a–d. Records were regionally compiled for the Antarctic Peninsula (**a**), West Antarctica (**b**), coastal East Antarctica (**c**) and the Antarctic Plateau (**d**) (see Methods). Central map shows the location of records according to environmental indicator (colours) and record type (symbols), as well as the boundaries of the four geographic regions (black lines), the 2,000-m elevation contour (grey curve), and the trend in sea-ice concentration over the 1979–2014 interval (shading). Within each region (**a–d**), records were compiled as 5-year averages (dark lines) according to the environmental parameter that they represent: observed surface air temperature (SAT) (red); proxy for SAT (orange); borehole inversion reconstruction of surface temperatures (greens); proxy for sea surface temperature (blue); and proxy for sea-ice conditions (cyan). Shadings (and thin vertical lines) denote ranges of estimates across records within each 5-year bin. The borehole temperature records are shown individually with uncertainty bounds (see Supplementary Fig. 4 for additional details). All records are expressed as temperature anomalies ($^{\circ}\text{C}$ units) or normalized data (σ -units) relative to 1960–1990. Details of datasets used in this figure are provided in Supplementary Table 1.

ocean profiles only since 2004 (ref. 7), and even now, few ocean profiles are obtained within the sea-ice zone.

Antarctic annual mean climate trends over the 1979–2014 interval covered by satellite observations (Fig. 1; see Supplementary Fig. 1 for location map) are dominated by statistically significant ($p < 0.05$) linear trends indicating: (1) an intensification of the mid-latitude westerly winds related to an increasing SAM index; (2) an overall sea surface temperature (SST) cooling, except in the southeast Indian Ocean sector, and in the Weddell, Bellingshausen and Amundsen Seas¹⁷ (not visible in Fig. 1 owing to sea-ice shading); (3) an overall expansion of sea ice, underpinned by a large increase in the Ross Sea sector, but partly offset by large decreases in the Amundsen–Bellingshausen sector, around the Antarctic Peninsula, and in the southeast Indian Ocean; (4) a strong surface air warming over the West Antarctic Ice Sheet (WAIS) and Antarctic Peninsula regions; and (5) surface air cooling above Adélie Land in East Antarctica. The surface air temperature (SAT) records from individual stations (inset panels in Fig. 1) demonstrate how considerable interannual to decadal variability underlies these long-term trends. In many cases, the annual-mean trends arise from strong trends in specific seasons (Supplementary Fig. 2).

Time series of summer anomalies in hemispherically averaged SST, zonal wind and sea-ice extent exhibit consistent multi-decadal variability since 1950 (ref. 17), suggesting that recent changes in multiple variables are strongly coupled. Many of the observed changes in SH high-latitude climate can be related to changes in atmospheric circulation. Strengthening of the westerly winds associated with the positive SAM trend causes spatially coherent changes in SAT over Antarctica¹⁸, and in particular can account for the summer warming over the eastern Antarctic Peninsula^{19,20}. Cooling of the surface ocean and warming of the subsurface ocean^{21–25} throughout the Southern Ocean can also be partly attributed to a westerly wind-forced increase in northward Ekman transport of cold sub-Antarctic surface waters. Summer trends in the SAM are distinct from natural variations²⁶, and are attributed to stratospheric ozone depletion, and the associated stratospheric cooling over Antarctica^{10,27}. In addition, regional atmospheric circulation changes led to warming trends in winter and spring, distinct from the summertime warming associated with the SAM, particularly over the WAIS and the western Antarctic Peninsula during the second half of the twentieth century^{11,28–32}. In the past 10–15 years, however, the rate of warming over the Peninsula has slowed markedly, in all seasons, but most strongly in summer (time series in Supplementary Fig. 2).

Table 1 | Summary of trend emergence analysis.

| | 50% of models exceeding control trends | | 90% of models exceeding control trends | | Direction |
|-----|----------------------------------------|----------------------|----------------------------------------|----------------------|-----------|
| | End year | Trend length (years) | End year | Trend length (years) | |
| SIE | 2031 | 53 | 2098 | 120 | Below |
| SST | 2021 | 43 | 2056 | 78 | Above |
| SAT | <2014 | <36 | 2050 | 72 | Above |
| SAM | 2015 | 37 | 2044 | 66 | Above |

Indicated are the end year (20YY) and trend length (in years) of 1979–20YY linear trends for which (left) 50% and (right) 90% of Historical-RCP8.5 simulated trends in CMIP5 models fall outside the 5–95% distribution (either above 95%, or below 5%) of pre-industrial trends of the same length in the same model.

Regional atmospheric circulation changes are also a potential driver of the recent trends in Antarctic sea ice³³, in particular through the strengthening of the Amundsen Sea Low (ASL)³⁴. Deepening of the ASL is linked to both changes in the SAM³⁵ and to atmospheric teleconnections with the tropical Pacific^{11,29,34,36,37}. The ASL has intensified onshore warm air flow over the Amundsen–Bellingshausen sector, and colder air flow offshore in the Ross Sea sector³⁸. This has contributed to the characteristic dipole of contrasting SAT and sea-ice concentration changes between the Ross Sea and the Amundsen–Bellingshausen/Antarctic Peninsula regions^{11,36,39,40}. An additional mechanism that may partly explain the overall increasing trend in Antarctic sea-ice extent (SIE) involves the increased meltwater input, which has contributed to freshening of the Southern Ocean (for example ref. 41), stabilization of the water column⁴² and thus potentially a reduction of the vertical ocean heat flux, enabling more prevalent sea ice formation^{43,44}.

Changes in SAT, atmospheric and ocean circulation have also affected the ice sheet itself, through surface melting of ice shelves around the Antarctic Peninsula⁴⁵, and melting of ice shelves from below owing to the intrusion of warm circumpolar deep water onto the continental shelf⁴⁶. The importance of the latter process is particularly evident along the margin of the WAIS^{47–49} and is associated with regional atmospheric circulation changes forced by teleconnections from the tropics^{48,50}.

The numerous interconnections between changes in the SH high-latitude atmosphere, ocean and sea-ice systems provide strong feedbacks that can amplify initial perturbations related, for instance, to winds or modifications in the hydrological cycle^{42,51,52}. These connections also demonstrate the need to assess the significance and impacts of SH high-latitude climate changes in a holistic way, using multiple variables.

Historical records and natural archives

To place these recent observed trends into a longer-term context, we compiled observational records of SAT longer than 55 years as well as proxy records for SAT, SST and sea ice, extracted from annually to multi-annually resolved ice and marine sediment cores, spanning the past 200 years (see Supplementary Table 1 for details of the datasets used, and Supplementary Methods for data compilation). Datasets were grouped into four different sectors, which were designed to group observational and proxy records with similar patterns of variability while also working within the constraints of data availability. Our regions comprised three near-coastal zones: (1) the Antarctic Peninsula region including the Bellingshausen and Scotia Seas, (2) the WAIS and the Ross Sea region, and (3) a broad region spanning coastal East Antarctica and incorporating the adjacent oceans and the Weddell Sea. The final region (4) is defined over the inland East Antarctic Plateau above 2,000 m elevation. The separation of coastal from inland regions reflects known differences in atmospheric transport dynamics pathways for weather events that impact inland versus coastal sites in Antarctica⁵³. Figure 2 shows these sectors and the data available for this synthesis, and highlights the paucity of climate information currently available for many parts of Antarctica.

Antarctic Peninsula sector. Of the four sectors, the Antarctic Peninsula has the longest observed SAT record (1903 to present); prior to the late 1940s, SAT is only available from the single Orcadas station, located northeast of the Peninsula itself. Instrumental data, proxy palaeotemperature records (ice cores and a moss bank core) and borehole temperature inversions show that the Antarctic Peninsula warming trend (Fig. 1) is part of a longer-term regional warming trend (Fig. 2a). The correspondence between instrumental and proxy data and between multiple proxy data sources may be stronger here than for any other region, suggesting that this is a robust context for the late twentieth-century temperature trend. The James Ross Island (JRI) ice core suggests that local warming began in the 1920s and has been statistically significant ($p < 0.1$) since the 1940s⁵⁴. Ice cores from the Gomez and Ferrigno sites and a moss bank core demonstrate that the twentieth-century rise in SAT on the northern Peninsula also extends south to the southwest Antarctic Peninsula^{55,56} and was accompanied by increases in snow accumulation^{57,58} and increased biological productivity, suggesting that temperature changes were likely to be year-round. Antarctic Peninsula warming has been related to intensification of the circumpolar westerlies in austral summer and autumn¹⁹, to associated deepening of the ASL, and to central tropical Pacific warming in austral autumn, winter and spring¹¹.

None of the most recent 36-year trends in the proxy SAT records is unprecedented relative to trends of the same length from earlier portions of the palaeoclimate archives (Supplementary Methods; Supplementary Fig. 3a). The most recent 100-year trends do exceed the upper 95% level of all earlier 100-year trends in three of the Antarctic Peninsula ice-core isotope records (JRI, Gomez and Ferrigno; Supplementary Fig. 3c); for the JRI core the most recent 100-year warming trend falls within the upper 0.3% of the distribution of all 100-year trends over the past 2,000 years^{54,59}.

Two marine SST proxy records from the northern Antarctic Peninsula show a warming trend over the twentieth century that was most prominent over roughly the 1920s to 1950s (Fig. 2a). A cooling trend in the most recent decades of the proxy stack appears to be of similar magnitude to earlier episodes of decadal-scale variability. In this sector, sea-ice information is derived from one historical record, three ice-core chemical records⁶⁰ and two marine diatom records spanning the Bellingshausen Sea and Scotia Sea/northern Weddell Sea. They depict a regionally coherent sea-ice decrease from the 1920s to the 1950s, coincident with proxy evidence for SST increases. The proxy composite does not clearly capture the Bellingshausen sea-ice decline observed by satellites since 1979, although individual studies have demonstrated that this recent observed decline is embedded within a longer-term decreasing trend that persisted through the twentieth century and was strongest at mid-century^{61,62}.

West Antarctica. In West Antarctica, SAT observations^{28,30}, a borehole temperature profile^{63,64} and ice-core water stable isotope records⁶⁵ all depict a consistent, statistically significant warming trend beginning in the 1950s. These trends are greatest in winter

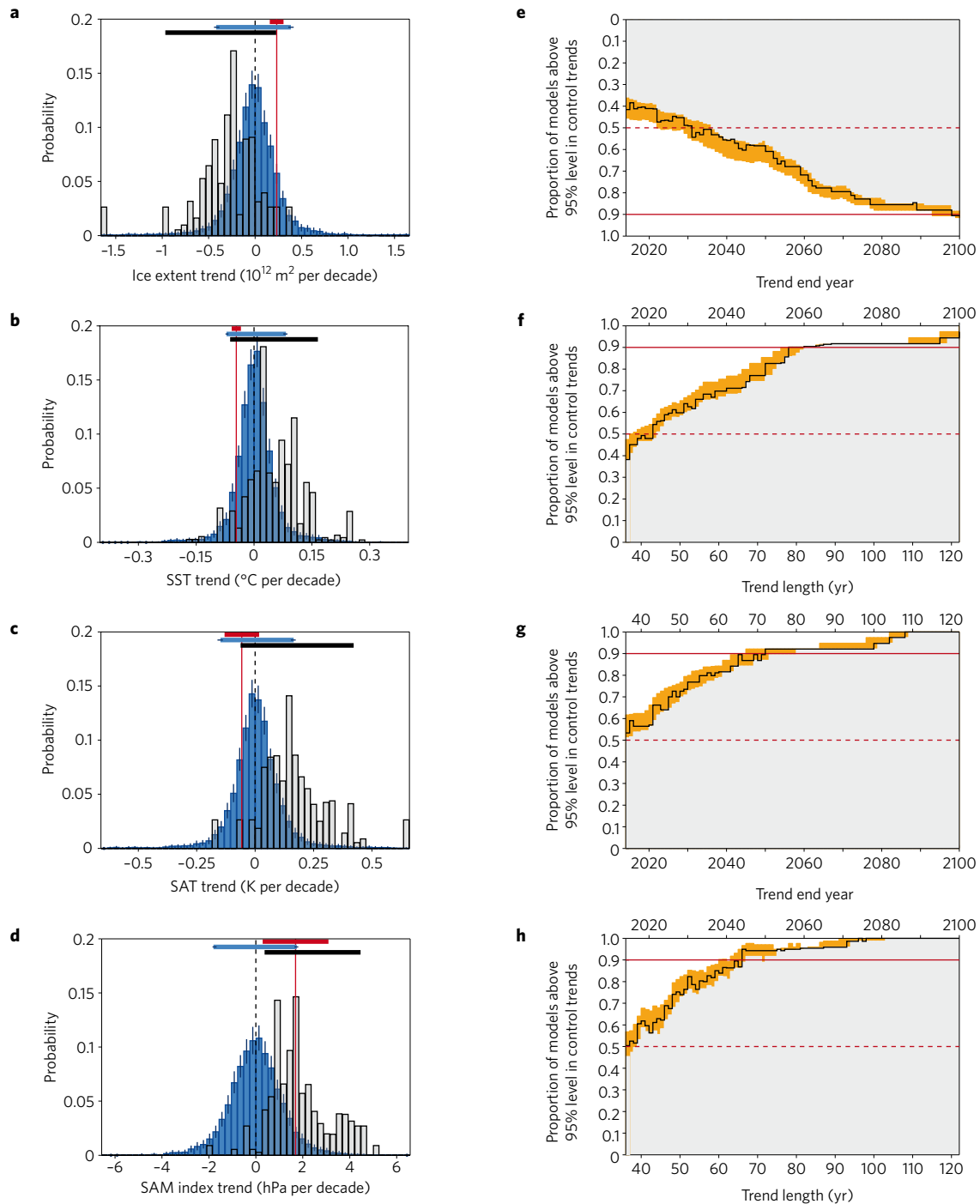


Figure 3 | Antarctic climate trends in CMIP5 simulations. a–d, Distributions of (blue) 36-year linear trends in an ensemble of CMIP5 pre-industrial simulations and (black/grey) 1979–2014 trends in an ensemble of CMIP5 historical (1979–2005)–RCP8.5 (2006–2014) simulations (see Supplementary Methods). Red vertical lines correspond to observed 36-year linear trends (1979–2014). Horizontal bars depict (red) the 90% confidence interval of the observed trend, (blue) the 5–95% range of the simulated pre-industrial distribution and (black) the 5–95% range of the simulated 1979–2014 trend distribution. The dark blue error bars on the pre-industrial histograms and horizontal ranges are 5–95% uncertainty intervals based on Monte Carlo analysis (see Methods). **e–h**, Proportion of CMIP5 model experiments whose linear trends starting in 1979 are above the 95% level (below the 5% level for panel **e**) of the distribution of trends of the same length in their matching control simulation. Simulations follow the RCP8.5 scenario after year 2005. Dashed and solid red lines highlight the 50% and 90% levels of the cumulative distributions (Table 1). The orange bars are 5–95% uncertainty ranges based on Monte Carlo analysis of equal length segments from the pre-industrial simulations (see Methods). Chosen climate variables are Southern Hemisphere sea-ice extent (**a,e**), mean SST south of 50° S (**b,f**), mean SAT south of 50° S (**c,g**) and SAM index (**d,h**). Model details are given in Supplementary Table 2. Observations used to compute observed sea-ice extent and SST trends over the 1979–2014 period are referenced in Fig. 1. The observed 1979–2014 SAT trend is derived from ERA-Interim 2-m air temperature fields. Modelled and observed SAM indices were calculated from annual mean time series using empirical orthogonal function analysis applied on 500-hPa geopotential height fields over the 90° S to 20° S region, with observation-based geopotential height fields taken from the ERA-Interim reanalysis.

and spring, and closely associated with the rapid decline in sea ice observed in the Amundsen–Bellingshausen Seas^{40,65,66}. The annual mean SAT trend over West Antarctica may be among the most rapid warming trends of the past few decades anywhere on Earth (2.2 ± 1.3 °C increase during 1958–2010 at Byrd Station, mostly owing to changes in austral winter and spring)^{30,67}. Nevertheless, the natural decadal variability in this region is also large, owing to the strong variability of the ASL⁶⁸, amplified by teleconnections with the tropical Pacific also during winter and spring^{11,29,69}. This differs markedly from the situation on the Antarctic Peninsula, where the summertime trends occur against a background of relatively small interannual variability³¹. As a consequence, the large recent trends cannot yet be demonstrated to be outside the range of natural variability (see, for example, 100-year trend analysis in Supplementary Fig. 3c). An analysis of more than 20 ice-core records from West Antarctica⁶⁵ concluded that the most recent decades were probably the warmest in the past 200 years, but with low confidence because of a similar-magnitude warming event during the 1940s associated with the major 1939–1942 El Niño event⁷⁰.

At present, no high-resolution reconstructions of SST or SIE are available for the Amundsen–Ross Sea sector to give context to the observed satellite-era trends there.

Coastal East Antarctica. No recent multi-decadal trend emerges from the compilation of SAT observations and proxy records in coastal East Antarctica. Recent fluctuations lie within the decadal variability documented from ice-core water isotope records, and recent 36-year and 100-year trends remain within the 5–95% range of earlier trends within each record (Supplementary Fig. 3a,c). The only available long-term borehole temperature reconstruction suggests a recent warming trend. This apparent contradiction may arise from spatial gradients and differences in recent temperature trends (for example Fig. 1) across this geographically extensive but data-sparse sector. Indeed, only seven meteorological stations, two ice-core water isotope records of sufficient resolution (see Supplementary Methods) and one 100-year borehole profile occupy a longitudinal region spanning 150° E to 40° W (Fig. 2a). Networks of isotope records from shallow ice cores (not compiled in this study owing to their limited temporal coverage) do provide evidence for a statistically significant increasing SAT trend in the past 30–60 years over the Fimbul Ice Shelf, East Antarctica⁷¹ and over Dronning Maud Land⁷², despite no observed warming at the nearby Neumayer station^{71,72}.

The single SST proxy record available from off the coast of Adélie Land⁷³ (Fig. 2) shows a strong increase post-1975, and, despite considerable decadal variability, the final 36-year trend exceeds the 95% range of trends in the full record (Supplementary Fig. 3a,c). Satellite observations, showing a regional SIE increase across this sector since 1979, are not mirrored by proxy records, which suggest an overall sea-ice decline since the 1950s⁷⁴, overlaid by strong decadal variability (Fig. 2). This also highlights the challenges in interpretation of sea-ice proxies, which can be sensitive to variations in sea-ice thickness, duration or local dynamics. For example, near the Mertz glacier, sea-ice proxy records spanning the past 250 years depict large multi-decadal variations that are attributed to iceberg calving events and are comparable to, or larger than, the most recent 36-year or 100-year trends⁷³ (Supplementary Fig. 3b,c).

East Antarctic Plateau. The stable isotope records for the East Antarctic Plateau do not show statistically significant trends in the final 36 years of their record (Supplementary Fig. 3a), unlike the observed SAT for the region (Fig. 1 inset b). Comparison of Figs 1 and 2 indicates that the stable water isotope records for the East Antarctic Plateau come from locations spanning differing temperature trends in Fig. 1. The Plateau Remote core on the central plateau is characterized by large decadal variability, and the most

recent 100-year trend remains well within the 5–95% range of earlier trends. Towards the margins of the East Antarctic Plateau, the EDML and Talos Dome ice cores display recent 100-year warming and cooling trends, respectively, that are significant with respect to earlier 100-year trends in these cores (Supplementary Fig. 3c). Temperature records from borehole inversions⁷⁵, which cannot resolve decadal variability, also show evidence for modest temperature increases on the Dronning Maud Land side of the East Antarctic Plateau during the late twentieth century, with warming apparently beginning earlier closer to the coast. The differing characteristics of long-term temperature variability and trends at sites across the Antarctic Plateau again highlight the importance of increasing the spatial coverage of proxy records from this data-sparse region.

The Southern Annular Mode. The history of the SAM over the past 200 years has been assessed in a number of previous reconstructions using syntheses of station observations^{26,76,77} and palaeoclimate networks^{18,78,79} (not shown). Reconstructions from station data display strong decadal variability and season-specific trends. The summer SAM exhibits the strongest post-1960s trend, which is assessed as unusual compared with trends in the earlier part of the century²⁶. A summer SAM index reconstructed from mid-latitude tree rings also indicates that the recent positive phase of the SAM is unprecedented in the context of at least the past 600 years⁷⁹. Similarly, an annual average SAM index reconstruction based on a network of temperature-sensitive palaeoclimate records spanning Antarctica and southern South America indicates that the SAM is currently in its most positive state over at least the past 1,000 years¹⁸. SAM index reconstructions display a steady⁷⁹ or declining¹⁸ SAM index since the early 1800s, reaching a minimum in the early to mid-twentieth century^{18,79}, before commencement of the positive SAM trend that is seen in observations (Fig. 1).

Simulated Antarctic climate trends and variability

The satellite observations and longer historical and proxy-based climate records reviewed in preceding sections reveal significant regional and seasonal climatic trends of both positive and negative signs and with a range of amplitudes, together with substantial decadal to centennial variability in the high-latitude SH. To further assess whether recent climate variations may be attributed to externally forced changes, or can be explained by unforced multi-decadal variability, we now examine statistics of 36-year trends in model simulations from CMIP5¹² and compare these to observed trends over the 1979–2014 period.

Trend distributions from pre-industrial control simulations provide an estimate of internally generated variability under fixed external forcing. The CMIP5 climate models display large internal multi-decadal variability in the high southern latitudes (Fig. 3), with satellite-era observational trends remaining within the 5–95% range of simulated internal variability for the annual means of all four examined variables — SIE, SST, SAT and the SAM index (Fig. 3a–d). Based on this comparison, the null hypothesis stating that the observed 1979–2014 trends are explained by internal climate system variability alone cannot be rejected at the 90% confidence level, with the underlying assumption that the simulated multi-decadal variability is of the correct magnitude. But a seasonal breakdown of observed and simulated trends reveals that observed SAM trends in summer and autumn exceed the 95% level of control variability (Supplementary Fig. 5), consistent with a dominant role of stratospheric ozone depletion in the recent shift toward positive SAM^{10,27}. The summer SAT trend also stands out as anomalously negative against the modelled pre-industrial variability (Supplementary Fig. 5).

In order to estimate the combined influence of the intrinsic variability of the SH climate system and the response to known historical (natural and anthropogenic) forcings, we next compare

statistics of modelled 1979–2014 trends in externally forced simulations against observations (see Supplementary Methods). With this measure of multi-model variability, the observed trends in SIE, SST and SAT appear only marginally consistent with the CMIP5 ensemble of simulated trajectories (Fig. 3a–c), in agreement with previous analyses^{44,80,81}. For instance, only 15% of model simulations exhibit sea-ice expansion over 1979–2014, and only 3% a larger SIE increase than that observed by satellites. Similarly, only 8% of models predict a negative trend in average SAT south of 50° S. In contrast, the likelihood of positive trends in the SAM index is increased in the externally forced simulations relative to unforced simulations, resulting in an improved agreement with the observed SAM trend (Fig. 3d).

Thus the statistics of 36-year trends are consistent with the hypothesis that anthropogenic forcing contributes to the recent positive SAM trend. Our comparisons also highlight the mismatch between CMIP5 historical simulations and observed recent trends in SIE and surface temperatures. We suggest that internal variability alone is unlikely to be sufficient to explain this mismatch. Indeed, the recent observed expansion of Antarctic sea ice and average surface cooling south of 50° S stand out as rare events when benchmarked against the ensemble of simulated trends for the 1979–2014 period (Fig. 3a–c).

Deficiencies in the model representation of SH climate are likely contributors to the disagreement between observations and forced climate simulations^{82,83}. Inaccurate or missing Earth system feedbacks in the CMIP5 simulations, such as the absence of the freshwater input due to ice-sheet mass loss, and unresolved physical processes, related to sea-ice rheology, thin ice properties, stratospheric processes, katabatic winds, ocean–ice shelf interactions and sub-grid-scale ocean processes, can bias both the simulated internal variability and the model response to external forcing. For example, subsurface ocean warming around Antarctica in response to strengthening of the SH westerly winds has been found to occur at twice the magnitude in a high-resolution ocean model compared with coarser CMIP5 simulations²². Comparisons of CMIP5 last-millennium simulations against palaeoclimate data have also shown deficiencies in the SH, indicating that CMIP5 models may underestimate the magnitude of unforced variability in the SH or overestimate the SH climate response to external forcing⁸⁴. Understanding the missing processes and the relationships between these processes and model skill will be crucial for future model developments in order to improve the model ability to simulate variability of the SH high-latitude climate and its response to forcing.

Within these limitations in the representation of SH high-latitude climate in the current generation of climate models, the available CMIP5 model output suggests that the observed and simulated 36-year (1979–2014) trends are not large enough to determine whether they are externally forced or merely a reflection of internal variability (Fig. 3a–d). Similarly, the most recent 36-year trends in the palaeoclimate records reviewed here are also too short to be considered unusual relative to the range of earlier 36-year trends in the past 200 years (Supplementary Fig. 3).

We further explore this by calculating the required duration of anthropogenically driven trends under the RCP8.5 scenario for SH high-latitude climate variables to emerge as statistically distinct from pre-industrial control variability. In a perfect model framework, this could be understood as estimating how long SH observations may need to be sustained before ongoing trends can be definitively attributed to anthropogenic climate change (Fig. 3e–h and Table 1).

For each model and variable, we assess whether the simulated trend starting in 1979 falls outside the matching 5–95% range of pre-industrial variability, and we calculate trends with lengths between 36 years (1979–2014) and 122 years (1979–2100). Our analysis reveals that, in 2015, over half of the models already simulate ‘unusual’ post-1979 trends in SAT and the SAM. For SST, 50%

of models have linear trends that emerge above unforced variability by 2021 (43-year trends), and for SIE the majority of CMIP5 models do not display trends emerging above the 95% significance level (relative to the pre-industrial distribution) until 2031 (that is, 53-year trends). For a trend emergence threshold of more than 90% of all CMIP5 models, trends do not emerge until between 2044 (66-year trends for SAM) and 2098 (120-year trends for SIE). Our results for the time of emergence of linear trends are in agreement with an earlier assessment using a different methodology⁸⁵, suggesting that the mid to high SH latitudes are among the last regions where the signal of anthropogenic forcing will be large enough to differentiate it from the range of natural variability. These CMIP5-based estimates may in fact underestimate the true length of time required for statistically distinct trends to emerge, if CMIP5 models underestimate the magnitude of internal variability or overestimate the forced climate response. Hence, notwithstanding known limitations in CMIP5 models, our analysis suggests that 36 years of observations are simply insufficient to interrogate and attribute trends in SH high-latitude surface climate.

Discussion

Climate change and variability over the high latitudes of the SH are characterized by strong regional and seasonal contrasts for all the variables investigated here. This is valid at interannual to decadal timescales, as illustrated in instrumental observations, as well as on longer timescales, as indicated in proxy-based reconstructions. The most unequivocal large-scale change over recent decades is the increase of the SAM index¹⁹ and the freshening and subsurface warming of the ocean^{23,24,41}. Regionally, a large warming has been observed over the Antarctic Peninsula and West Antarctic regions across the past 50 years. SIE has decreased in the Amundsen–Bellingshausen Seas while it has increased in the Ross Sea sector since 1979.

The large multi-decadal variations seen in high-resolution proxy-based reconstructions of temperature and SIE also have clear regional contrasts. Some estimates suggest common signals over the whole Southern Ocean, such as the decrease of the ice extent between the 1950s and the late 1970s deduced from whaling records (for example refs 86–88), but this remains to be confirmed by the analysis of additional observations. The longer records independently support the conclusion that most of the recent changes for any single variable largely result from natural variability and are not unprecedented over the past two centuries. This is consistent with results from state-of-the-art climate models showing that, except for the SAM index, most recent changes remain in the range of large-scale simulated internal variability. When analysing specifically the 1979–2014 period, including forced changes and internal variability, models struggle to track the observed trends in SST, SAT and sea-ice cover. This suggests either that a singular event associated with internal variability has been able to overwhelm the forced response in observations, or that CMIP5 models overestimate the forced response (potentially partly because of key processes missing in the models), or a combination of both.

Recent observations and process understanding of the atmosphere, sea ice, ocean and ice sheets suggest strong coupling, which means that investigations need to encompass and understand the dynamics of the whole climate system. Statistics independently applied to a few large-scale metrics may not allow a robust comparison between observed and simulated trends. Regional and seasonal complexity⁸⁹ as well as physical relationships between different climate variables must be taken into account to evaluate the overall consistency of observed and modelled time-evolving climate states, and to identify caveats. We advocate process-oriented studies in which the primary mechanisms behind modelled behaviour are identified and their plausibility evaluated against available observations and theory.

In particular, the accelerating melting and calving of Antarctic ice shelves^{46,90,91} could have a pronounced influence on the recent and future evolution of the high-latitude Southern Ocean^{41,43,92–94}. Understanding and quantifying the role of changing glacial discharge in past and ongoing climatic trends is an important unresolved question requiring attention.

To improve the sampling of forced and natural variability for the recent period, we also emphasize the importance of considering multiple models, as well as multiple realizations of different models. In this sense, large ensembles, such as those recently released by some modelling groups⁹⁵, are particularly useful for improving estimates of internal variability compared with forced signals.

Atmospheric reanalyses are strongly dependent on the prescribed surface boundary conditions that are particularly uncertain before the 1970s in the Southern Ocean⁹⁶ and therefore have limited skills prior to the satellite era. Alternative approaches involve assimilation methods using proxy records and climate simulations in order to best reconstruct the past state of the Antarctic atmospheric circulation. Coupled ocean–sea-ice–atmosphere reanalysis⁹⁷, with specific attention to the high latitudes of the Southern Ocean, should thus be a target for the future. Preliminary studies have demonstrated the feasibility of this approach for ensuring the consistency between the various components of the system and the study of their interactions⁹⁸.

Our synthesis has emphasized that less than 40 years of instrumental climate data is insufficient to characterize the variability of the high southern latitudes or to robustly identify an anthropogenic contribution, except for the changes in the SAM. Although temperature changes over 1950–2008 from the average of individual stations have been attributed to anthropogenic causes⁹⁹, only low confidence can be assigned, owing to observational uncertainties¹⁰⁰ and large-scale decadal and multi-decadal variability. Detection and attribution studies depend on the validity of estimates of natural variability from climate model simulations. This is particularly the case for variables such as Antarctic sea ice, which have problematic representation in climate models³⁶ and short observational time series from which to estimate real multi-decadal variability. The strong regional variability on all timescales implies that the sparsity of observations and proxy data is a clear limitation, especially in the ocean, and that averaging climate properties over the entire Antarctic or Southern Ocean potentially aliases the regional differences.

The Antarctic climate system is strongly coupled, and future investigations need to combine information from different climate variables to identify the causes and mechanisms driving SH high-latitude climate variations. Process studies are essential to this task, along with a continued effort to maintain current observations from stations and satellites, and to expand the observational network in undocumented areas. The rescue of historical data is also critical to obtain a longer perspective. New high-resolution proxy data should be collected, both by expanding existing data types (for example lake sediments and deep-sea sediments) and by investing in new records such as moss banks. Improved spatial coverage of ice-core records and a requirement for a minimum suite of information from these archives (for example accumulation, water isotopes, borehole temperatures) are desirable, together with multiple records allowing improvement of the signal-to-noise ratio. Improved calibration of these proxy records (for example, water stable isotopes against temperature) is critical for the uncertainties associated with past temperature reconstructions. Progress is expected from the use of historical data, but also through improved proxy modelling, for example by incorporating water stable isotopes in high-resolution atmospheric models and quantifying post-deposition effects. Not least important is the use of nonlinear statistical analysis tools to improve the statistical analysis of observations and proxy data as well as model output evaluation. Gathering, utilizing, combining and improving the interpretation of data from all available sources

are imperative to understand recent climate changes in this data-sparse, but climatically important, region.

Received 29 February 2016; accepted 29 June 2016; published online 28 September 2016

References

- Church, J. A. *et al.* in *Climate Change 2013: The Physical Science Basis* (eds Stocker, T. F. *et al.*) Ch. 13 (IPCC, Cambridge Univ. Press, 2013).
- Bindschadler, R. A. *et al.* Ice-sheet model sensitivities to environmental forcing and their use in projecting future sea level (the SeaRISE project). *J. Glaciol.* **59**, 195–224 (2013).
- Ritz, C. *et al.* Potential sea-level rise from Antarctic ice-sheet instability constrained by observations. *Nature* **528**, 115–118 (2015).
- Majkut, J. D. *et al.* An observing system simulation for Southern Ocean carbon dioxide uptake. *Phil. Trans. R. Soc. A* **372**, 20130046 (2014).
- Landschutzer, P. *et al.* The reinvigoration of the Southern Ocean carbon sink. *Science* **349**, 1221–1224 (2015).
- Rhein, M. *et al.* in *Climate Change 2013: The Physical Science Basis* (eds Stocker, T. F. *et al.*) Ch. 3 (IPCC, Cambridge Univ. Press, 2013).
- Roemmich, D. *et al.* Unabated planetary warming and its ocean structure since 2006. *Nat. Clim. Change* **5**, 240–245 (2015).
- Levitus, S. *et al.* World ocean heat content and thermosteric sea level change (0–2000 m), 1955–2010. *Geophys. Res. Lett.* **39**, L10603 (2012).
- Thompson, D. W. J. & Wallace, J. M. Annular modes in the extratropical circulation. Part I: Month-to-month variability. *J. Clim.* **13**, 1000–1016 (2000).
- Thompson, D. W. J. *et al.* Signatures of the Antarctic ozone hole in Southern Hemisphere surface climate change. *Nat. Geosci.* **4**, 741–749 (2011).
- The stratospheric ozone hole in the Southern Hemisphere has led to a strengthening of westerly winds in austral summer (that is, a positive Southern Annular Mode), leading to a range of surface climate impacts.**
- Ding, Q., Steig, E. J., Battisti, D. S. & Kuettel, M. Winter warming in West Antarctica caused by central tropical Pacific warming. *Nat. Geosci.* **4**, 398–403 (2011).
- Taylor, K. E., Stouffer, R. J. & Meehl, G. A. An overview of CMIP5 and the experiment design. *Bull. Am. Meteorol. Soc.* **93**, 485–498 (2012).
- Eisenman, I., Meier, W. N. & Norris, J. R. A spurious jump in the satellite record: has Antarctic sea ice expansion been overestimated? *Cryosphere* **8**, 1289–1296 (2014).
- Cavaliere, D. J., Parkinson, C. L. & Vinnikov, K. Y. 30-year satellite record reveals contrasting Arctic and Antarctic decadal sea ice variability. *Geophys. Res. Lett.* **30**, 1970 (2003).
- Meier, W. N., Gallaher, D. & Campbell, G. G. New estimates of Arctic and Antarctic sea ice extent during September 1964 from recovered Nimbus I satellite imagery. *Cryosphere* **7**, 699–705 (2013).
- Gallaher, D. W., Campbell, G. G. & Meier, W. N. Anomalous variability in Antarctic sea ice extents during the 1960s with the use of Nimbus data. *IEEE J. Sel. Topics Appl. Earth Obs. Remote Sens.* **7**, 881–887 (2014).
- Fan, T., Deser, C. & Schneider, D. P. Recent Antarctic sea ice trends in the context of Southern Ocean surface climate variations since 1950. *Geophys. Res. Lett.* **41**, 2419–2426 (2014).
- Abram, N. J. *et al.* Evolution of the Southern Annular Mode during the past millennium. *Nat. Clim. Change* **4**, 564–569 (2014).
- The SAM index has undergone large centennial variability, with a progressive shift towards a positive phase since the fifteenth century.**
- Thompson, D. W. J. & Solomon, S. Interpretation of recent Southern Hemisphere climate change. *Science* **296**, 895–899 (2002).
- Marshall, G. J. Half-century seasonal relationships between the Southern Annular Mode and Antarctic temperatures. *Int. J. Climatol.* **27**, 373–383 (2007).
- Sen Gupta, A. & England, M. H. Coupled ocean–atmosphere–ice response to variations in the Southern Annular Mode. *J. Clim.* **19**, 4457–4486 (2006).
- Spence, P. *et al.* Rapid subsurface warming and circulation changes of Antarctic coastal waters by poleward shifting winds. *Geophys. Res. Lett.* **41**, 4601–4610, (2014).
- Gille, S. T. Decadal-scale temperature trends in the Southern Hemisphere ocean. *J. Clim.* **21**, 4749–4765 (2008).
- Schmidtke, S., Heywood, K. J., Thompson, A. F. & Aoki, S. Multidecadal warming of Antarctic waters. *Science* **346**, 1227–1231 (2014).
- Ferreira, D., Marshall, J., Bitz, C. M., Solomon, S. & Plumb, A. Antarctic Ocean and sea ice response to ozone depletion: a two-time-scale problem. *J. Clim.* **28**, 1206–1226 (2015).
- Fogt, R. L. *et al.* Historical SAM variability. Part II: Twentieth-century variability and trends from reconstructions, observations, and the IPCC AR4 Models. *J. Clim.* **22**, 5346–5365 (2009).
- Simulations from IPCC AR4 models did not fully capture the observed natural variability in the SAM, although they are reasonably successfully at capturing the strong summertime trends since 1957.**

27. Gillett, N. P. & Thompson, D. W. J. Simulation of recent Southern Hemisphere climate change. *Science* **302**, 273–275 (2003).
28. Steig, E. J. *et al.* Warming of the Antarctic ice-sheet surface since the 1957 International Geophysical Year. *Nature* **457**, 459–462 (2009).
29. Ding, Q., Steig, E. J., Battisti, D. S. & Wallace, J. M. Influence of the tropics on the Southern Annular Mode. *J. Clim.* **25**, 6330–6348 (2012).
30. Bromwich, D. H. *et al.* Central West Antarctica among the most rapidly warming regions on Earth. *Nat. Geosci.* **6**, 139–145 (2013).
31. Ding, Q. & Steig, E. J. Temperature change on the Antarctic Peninsula linked to the tropical Pacific. *J. Clim.* **26**, 7570–7585 (2013).
32. Clem, K. R. & Fogt, R. L. South Pacific circulation changes and their connection to the tropics and regional Antarctic warming in austral spring, 1979–2012. *J. Geophys. Res. Atmos.* **120**, 2773–2792 (2015).
33. Holland, P. R. & Kwok, R. Wind-driven trends in Antarctic sea-ice drift. *Nat. Geosci.* **5**, 872–875 (2012).
34. Raphael, M. *et al.* The Amundsen Sea Low: variability, change and impact on Antarctic Climate. *Bull. Am. Meteorol. Soc.* **97**, 111–121 (2016).
35. Turner, J., Phillips, T., Hosking, J. S., Marshall, G. J. & Orr, A. The Amundsen Sea Low. *Int. J. Climatol.* **33**, 1818–1829 (2013).
36. Turner, J., Hosking, J. S., Bracegirdle, T. J., Marshall, G. J. & Phillips, T. Recent changes in Antarctic Sea Ice. *Phil. Trans. R. Soc. A* **373**, 20140163 (2015).
37. Fogt, R. L. & Wovrosh, A. J. The relative influence of tropical sea surface temperatures and radiative forcing on the Amundsen Sea Low. *J. Clim.* **28**, 8540–8555 (2015).
38. Hosking, J. S., Orr, A., Marshall, G. J., Turner, J. & Phillips, T. The influence of the Amundsen–Bellingshausen seas low on the climate of West Antarctica and its representation in coupled climate model simulations. *J. Clim.* **26**, 6633–6648 (2013).
39. Stammerjohn, S. E., Martinson, D. G., Smith, R. C., Yuan, X. & Rind, D. Trends in Antarctic annual sea ice retreat and advance and their relation to El Niño–Southern Oscillation and Southern Annular Mode variability. *J. Geophys. Res. Oceans* **113**, C03S90 (2008).
40. Schneider, D. P., Deser, C. & Okumura, Y. An assessment and interpretation of the observed warming of West Antarctica in the austral spring. *Clim. Dynam.* **38**, 323–347 (2012).
41. Rye, C. D. *et al.* Rapid sea-level rise along the Antarctic margins in response to increased glacial discharge. *Nat. Geosci.* **7**, 732–735 (2014).
42. de Lavergne, C., Palter, J. B., Galbraith, E. D., Bernardello, R. & Marinov, I. Cessation of deep convection in the open Southern Ocean under anthropogenic climate change. *Nat. Clim. Change* **4**, 278–282 (2014).
43. Bintanja, R., van Oldenborgh, G. J., Drijfhout, S. S., Wouters, B. & Katsman, C. A. Important role for ocean warming and increased ice-shelf melt in Antarctic sea-ice expansion. *Nat. Geosci.* **6**, 376–379 (2013).
- As a result of basal melting of Antarctic ice shelves, a layer of cool, fresh meltwater in the surface ocean around Antarctica increases stratification, and according to some model simulations this may have contributed to the recent expansion of sea-ice extent, although the magnitude of this effect is uncertain.**
44. Swart, N. C. & Fyfe, J. C. The influence of recent Antarctic ice sheet retreat on simulated sea ice area trends. *Geophys. Res. Lett.* **40**, 4328–4332 (2013).
45. Scambos, T. A., Hulbe, C., Fahnestock, M. & Bohlander, J. The link between climate warming and break-up of ice shelves in the Antarctic Peninsula. *J. Glaciol.* **46**, 516–530 (2000).
46. Pritchard, H. D. *et al.* Antarctic ice-sheet loss driven by basal melting of ice shelves. *Nature* **484**, 502–505 (2012).
47. Jenkins, A. *et al.* Observations beneath Pine Island Glacier in West Antarctica and implications for its retreat. *Nat. Geosci.* **3**, 468–472 (2010).
48. Dutrieux, P. *et al.* Strong sensitivity of Pine Island ice-shelf melting to climatic variability. *Science* **343**, 174–178 (2014).
49. Jacobs, S. S., Jenkins, A., Giulivi, C. F. & Dutrieux, P. Stronger ocean circulation and increased melting under Pine Island Glacier ice shelf. *Nat. Geosci.* **4**, 519–523 (2011).
50. Steig, E. J., Ding, Q., Battisti, D. S. & Jenkins, A. Tropical forcing of Circumpolar Deep Water Inflow and outlet glacier thinning in the Amundsen Sea Embayment, West Antarctica. *Ann. Glaciol.* **53**, 19–28 (2012).
51. Kirkman, C. H. & Bitz, C. M. The effect of the sea ice freshwater flux on Southern Ocean temperatures in CCSM3: deep-ocean warming and delayed surface warming. *J. Clim.* **24**, 2224–2237 (2011).
52. Goosse, H. & Zunz, V. Decadal trends in the Antarctic sea ice extent ultimately controlled by ice–ocean feedback. *Cryosphere* **8**, 453–470 (2014).
53. King, J. C. & Turner, J. T. *Antarctic Meteorology and Climatology* (Cambridge Univ. Press, 1997).
54. Abram, N. J. *et al.* Acceleration of snow melt in an Antarctic Peninsula ice core during the twentieth century. *Nat. Geosci.* **6**, 404–411 (2013).
55. Thomas, E. R., Dennis, P. F., Bracegirdle, T. J. & Franzke, C. Ice core evidence for significant 100-year regional warming on the Antarctic Peninsula. *Geophys. Res. Lett.* **36**, L20704 (2009).
56. Thomas, E. R., Bracegirdle, T. J., Turner, J. & Wolff, E. W. A 308 year record of climate variability in West Antarctica. *Geophys. Res. Lett.* **40**, 5492–5496 (2013).
57. Thomas, E. R., Marshall, G. J. & McConnell, J. R. A doubling in snow accumulation in the western Antarctic Peninsula since 1850. *Geophys. Res. Lett.* **35**, L01706 (2008).
58. Thomas, E. R., Hosking, J. S., Tuckwell, R. R., Warren, R. A. & Ludlow, E. C. Twentieth century increase in snowfall in coastal West Antarctica. *Geophys. Res. Lett.* **42**, 9387–9393 (2015).
59. Mulvaney, R. *et al.* Recent Antarctic Peninsula warming relative to Holocene climate and ice-shelf history. *Nature* **489**, 141–144 (2012).
60. Abram, N. J., Wolff, E. W. & Curran, M. A. J. A review of sea ice proxy information from polar ice cores. *Quat. Sci. Rev.* **79**, 168–183 (2013).
61. Abram, N. J. *et al.* Ice core evidence for a 20th century decline of sea ice in the Bellingshausen Sea, Antarctica. *J. Geophys. Res. Atmos.* **115**, D23101 (2010).
62. Murphy, E. J., Clarke, A., Abram, N. J. & Turner, J. Variability of sea-ice in the northern Weddell Sea during the 20th century. *J. Geophys. Res. Oceans* **119**, 4549–4572 (2014).
63. Orsi, A. J., Cornuelle, B. D. & Severinghaus, J. P. Little Ice Age cold interval in West Antarctica: evidence from borehole temperature at the West Antarctic Ice Sheet (WAIS) Divide. *Geophys. Res. Lett.* **39**, L09710 (2012).
64. Steig, E. J. & Orsi, A. J. The heat is on in Antarctica. *Nat. Geosci.* **6**, 87–88 (2013).
65. Steig, E. J. *et al.* Recent climate and ice-sheet changes in West Antarctica compared with the past 2,000 years. *Nat. Geosci.* **6**, 372–375 (2013).
- Temperatures have increased significantly in West Antarctica during the past 50 years but similar or higher temperatures have probably occurred in the past 2,000 years.**
66. Kuettel, M., Steig, E. J., Ding, Q., Monaghan, A. J. & Battisti, D. S. Seasonal climate information preserved in West Antarctic ice core water isotopes: relationships to temperature, large-scale circulation, and sea ice. *Clim. Dynam.* **39**, 1841–1857 (2012).
67. Bromwich, D. H. *et al.* Corrigendum: Central West Antarctica among the most rapidly warming regions on Earth. *Nat. Geosci.* **7**, 76–76 (2014).
68. Connolley, W. M. Variability in annual mean circulation in southern high latitudes. *Clim. Dynam.* **13**, 745–756 (1997).
69. Lachlan-Cope, T. & Connolley, W. Teleconnections between the tropical Pacific and the Amundsen–Bellingshausen Sea: role of the El Niño/Southern Oscillation. *J. Geophys. Res. Atmos.* **111**, D23101 (2006).
70. Schneider, D. P. & Steig, E. J. Ice cores record significant 1940s Antarctic warmth related to tropical climate variability. *Proc. Natl Acad. Sci. USA* **105**, 12154–12158 (2008).
71. Schlosser, E. *et al.* Recent climate tendencies on an East Antarctic ice shelf inferred from a shallow firn core network. *J. Geophys. Res. Atmos.* **119**, 6549–6562 (2014).
72. Altnau, S., Schlosser, E., Isaksson, E. & Divine, D. Climatic signals from 76 shallow firn cores in Dronning Maud Land, East Antarctica. *Cryosphere* **9**, 925–944 (2015).
73. Campagne, P. *et al.* Glacial ice and atmospheric forcing on the Mertz Glacier Polynya over the past 250 years. *Nat. Commun.* **6**, 1–9 (2015).
74. Curran, M. A. J., van Ommen, T. D., Morgan, V. I., Phillips, K. L. & Palmer, A. S. Ice core evidence for Antarctic sea ice decline since the 1950s. *Science* **302**, 1203–1206 (2003).
75. Muto, A., Scambos, T. A., Steffen, K., Slater, A. G. & Clow, G. D. Recent surface temperature trends in the interior of East Antarctica from borehole firn temperature measurements and geophysical inverse methods. *Geophys. Res. Lett.* **38**, L15502 (2011).
76. Jones, J. M. *et al.* Historical SAM Variability. Part I: Century-length seasonal reconstructions. *J. Clim.* **22**, 5319–5345 (2009).
77. Visbeck, M. A station-based Southern Annular Mode index from 1884 to 2005. *J. Clim.* **22**, 940–950 (2009).
78. Jones, J. M. & Widmann, M. Instrument- and tree-ring-based estimates of the Antarctic oscillation. *J. Clim.* **16**, 3511–3524 (2003).
79. Villalba, R. *et al.* Unusual Southern Hemisphere tree growth patterns induced by changes in the Southern Annular Mode. *Nat. Geosci.* **5**, 793–798 (2012).
80. Zunz, V., Goosse, H. & Massonnet, F. How does internal variability influence the ability of CMIP5 models to reproduce the recent trend in Southern Ocean sea ice extent? *Cryosphere* **7**, 451–468 (2013).
81. Shu, Q., Song, Z. & Qiao, F. Assessment of sea ice simulations in the CMIP5 models. *Cryosphere* **9**, 399–409 (2015).
82. Purich, A. P., Cai, W., England, M. H. & Cowan, T. Evidence for link between modelled trends in Antarctic sea ice and underestimated westerly wind changes. *Nat. Commun.* **7**, 1–9 (2016).
83. Notz, D. How well must climate models agree with observations? *Phil. Trans. R. Soc. A* **373**, 20140164 (2015).

84. Bothe, O. *et al.* Continental-scale temperature variability in PMIP3 simulations and PAGES 2k regional temperature reconstructions over the past millennium. *Clim. Past* **11**, 1673–1699 (2015).
Assessments of palaeoclimate data records and model simulations suggest consistency in the Northern Hemisphere but disagreement in the Southern Hemisphere, where models may underestimate the magnitude of internal variability or overestimate the response to external forcing.
85. Hawkins, E. & Sutton, R. Time of emergence of climate signals. *Geophys. Res. Lett.* **39**, L01702 (2012).
86. de la Mare, W. K. Whaling records and changes in Antarctic sea ice: consistency with historical records. *Polar Record* **38**, 355–358 (2002).
87. de la Mare, W. K. Changes in Antarctic sea-ice extent from direct historical observations and whaling records. *Clim. Change* **92**, 461–493 (2009).
88. Cotte, C. & Guinet, C. Historical whaling records reveal major regional retreat of Antarctic sea ice. *Deep-Sea Res. Part I: Oceanogr. Res. Pap.* **54**, 243–252 (2007).
89. Hobbs, W. R., Bindoff, N. L. & Raphael, M. N. New perspectives on observed and simulated Antarctic sea ice extent trends using optimal fingerprinting techniques. *J. Clim.* **28**, 1543–1560 (2015).
90. Rignot, E., Jacobs, S., Mouginot, J. & Scheuchl, B. Ice-shelf melting around Antarctica. *Science* **341**, 266–270 (2013).
91. Paolo, F. S., Fricker, H. A. & Padman, L. Volume loss from Antarctic ice shelves is accelerating. *Science* **348**, 327–331 (2015).
92. Swingedouw, D. *et al.* Antarctic ice-sheet melting provides negative feedbacks on future climate warming. *Geophys. Res. Lett.* **35**, L17705 (2008).
93. Hellmer, H. H., Kauker, F., Timmermann, R., Determann, J. & Rae, J. Twenty-first-century warming of a large Antarctic ice-shelf cavity by a redirected coastal current. *Nature* **485**, 225–228 (2012).
94. Fogwill, C. J., Phipps, S. J., Turney, C. S. M. & Golleger, N. R. Sensitivity of the Southern Ocean to enhanced regional Antarctic ice sheet meltwater input. *Earth's Future* **3**, 317–329 (2015).
95. Kay, J. E. *et al.* The Community Earth System Model (CESM) Large Ensemble Project: a community resource for studying climate change in the presence of internal climate variability. *Bull. Am. Meteorol. Soc.* **96**, 1333–1349 (2015).
96. Rayner, N. A. *et al.* Global analyses of sea surface temperature, sea ice, and night marine air temperature since the late nineteenth century. *J. Geophys. Res. Atmos.* **108**, 4407 (2003).
97. Laloyaux, P., Balmaseda, M., Dee, D., Mogensen, K. & Janssen, P. A coupled data assimilation system for climate reanalysis. *Q. J. R. Soc.* **142**, 65–78 (2016).
98. Goosse, H., Lefebvre, W., de Montety, A., Crespin, E. & Orsi, A. H. Consistent past half-century trends in the atmosphere, the sea ice and the ocean at high southern latitudes. *Clim. Dynam.* **33**, 999–1016 (2009).
99. Gillett, N. P. *et al.* Attribution of polar warming to human influence. *Nat. Geosci.* **1**, 750–754 (2008).
100. Bindoff, N. L. *et al.* in *Climate Change 2013: The Physical Science Basis* (eds Stocker, T. F. *et al.*) Ch. 10 (IPCC, Cambridge Univ. Press, 2013).

Acknowledgements

We thank H. Diamond, I. Goodwin, J. McClean, J. Twedt, J. Severinghaus, C. Wilkinson, R. Wilson and U. Zajaczkowski for their contributions to the meeting at which this paper was planned. The meeting and this project were supported by the Climate and Cryosphere project of the World Climate Research Programme (through the Polar Climate Predictability Initiative) and the Government of Canada through the Federal Department of the Environment. We also thank Past Global Changes (PAGES) for supporting this meeting; D. McCutcheon for producing Supplementary Fig. 1; the SCAR-Reader project for providing the Antarctic station data; J. Nicolas and D. Bromwich for making the Antarctic surface temperature reconstruction available; the National Snow

and Ice Data Centre for provision of the sea-ice data; the ECMWF for providing the Era Interim reanalysis; and NOAA for providing the SST data. We thank the many scientists who made their published palaeoclimate datasets available via public data repositories or personal requests, and we acknowledge the efforts of the PAGES Antarctica 2k working group in compiling many of the palaeoclimate records used in this study. We acknowledge the World Climate Research Programme's Working Group on Coupled Modelling, which is responsible for CMIP. The US Department of Energy's Program for Climate Model Diagnosis and Intercomparison provides coordinating support for CMIP and led the development of software infrastructure in partnership with the Global Organization for Earth System Science Portals.

Support was provided by the following organizations: N.J.A. QEII fellowship and Discovery Project awarded by the Australian Research Council (ARC DP110101161 and DP140102059); M.H.E., ARC Laureate Fellowship (FL100100214); V.M.D., Agence Nationale de la Recherche, project ANR-14-CE01-0001 (ASUMA), and logistical support to French Antarctic studies from the Institut Polaire Paul-Emile Victor (IPEV); B.S., PAGES Antarctica 2k and the ESF-PolarClimate HOLOCLIP project; H.G., the Fonds National de la Recherche Scientifique (F.R.S.-FNRS-Belgium), where he is Research Director; P.O.C., research grant ANPCyT PICT2012 2927; R.L.E., NSF grant 1341621; E.J.S., the Leverhulme Trust; S.T.G., NSF grants OCE-1234473 and PLR-1425989; D.P.S., NSF grant 1235231; NCAR is sponsored by the National Science Foundation (NSF); G.R.S., NSF grants AGS-1206120 and AGS-1407360; D.S., the French ANR CEPS project Green Greenland (ANR-10-CEPL-0008); G.J.M., UK Natural Environment Research Council (NERC) through the British Antarctic Survey research programme Polar Science for Planet Earth; A.K.M., US Department of Energy under contract DE-SC0012457; K.R.C., VUW doctoral scholarship; L.M.F., Australian Research Council (FL100100214); D.J.C., NERC grant NE/H014896/1; C.d.L., UPMC doctoral scholarship; A.J.O., EU grant FP7-PEOPLE-2012-IIF 331615; X.C., the French ANR CLIMICE (ANR-08-CEXC-012-01) and the FP7 PAST4FUTURE (243908) projects; J.A.R., Marsden grant VUW1408; I.E., NSF grant OCE-1357078; T.R.V., the Australian Government's Cooperative Research Centres programme, through the ACE CRC.

Author contributions

All authors conceived the paper. J.M.J., H.G. and S.T.G. organized the contributions to the manuscript, and contributed to writing and editing the manuscript. Observational data: G.R.S. undertook data analysis and figure preparation (Fig. 1 and Supplementary Fig. 2), which included contributions from M.H.E., E.J.S. and G.J.M.; M.H.E., G.R.S., J.A.R., R.L.F., M.N.R., G.J.M., D.P.S., I.E., P.O.C. and K.R.C. all contributed to discussions of analysis design, and to writing and revising the Antarctic climate monitoring section, and associated methods. Palaeoclimate and historical data: N.J.A. undertook the data compilation, with data contributions from B.S., A.J.O., X.C., P.O.C. and D.J.C. N.J.A. and T.R.V. prepared the figures (Fig. 2 and Supplementary Figs 3 and 4). T.R.V., N.J.A., P.O.C., D.J.C., X.C., V.M.D., A.J.O., E.J.S. and B.S. all contributed to discussions of analysis design, and to writing and revising the section on historical records and natural archives, and associated methods. Climate simulations: D.S. undertook coordination, D.S., C.d.L., N.J.A., A.K.M. and L.M.F. undertook data analysis, and C.d.L. and N.J.A. prepared the figures (Fig. 3 and Supplementary Fig. 5). D.S., N.J.A., M.H.E., L.M.F., C.d.L. and A.K.M. all contributed to discussions of analysis design, and to writing and revising the section on simulated Antarctic climate trends and variability, and associated methods. All authors reviewed the full manuscript.

Additional information

Supplementary information is available in the [online version of the paper](#). Reprints and permissions information is available online at www.nature.com/reprints. Correspondence should be addressed to J.M.J.

Competing financial interests

The authors declare no competing financial interests.

Assessing recent trends in high-latitude Southern Hemisphere surface climate

Julie. M. Jones^{*}, Sarah T. Gille, Hugues Goosse, Nerilie J. Abram, Pablo O. Canziani, Dan J. Charman, Kyle R. Clem, Xavier Crosta, Casimir de Lavergne, Ian Eisenman, Matthew H. England, Ryan L. Fogt, Leela M. Frankcombe, Gareth J. Marshall, Valérie Masson-Delmotte, Adele K. Morrison, Anaïs J. Orsi, Marilyn N. Raphael, James A. Renwick, David P. Schneider, Graham R. Simpkins, Eric J. Steig, Barbara Stenni, Didier Swingedouw and Tessa R. Vance.

e-mail: julie.jones@sheffield.ac.uk^{*}

This PDF contains data and methods, supplementary Tables 1-2, and supplementary Figures 1-5.

Data and Methods

Antarctic Climate Monitoring

Figure 1 and Supplementary Figure 2

We used station-based (shaded shapes) and reconstruction-based (shading over Antarctica) temperature data to calculate Antarctic surface air temperature (SAT) trends over the period 1979-2014. Regional SAT was calculated by averaging the station-based temperatures for each respective region denoted by shaded shapes. Only Byrd station is available for West Antarctica; thus only one line is provided for that region. Station-based temperature data are from the quality-controlled SCAR READER (Scientific Committee on Antarctic Research REference Antarctic Data for Environmental Research) Project¹, and the reconstructed data are from the Ohio State University Byrd Polar Research Center's Reconstruction of Antarctic near-surface temperature dataset². Reconstructed temperature data span the period 1979-2012, and trends were scaled to represent the period 1979-2014.

Sea surface temperature (SST) trends (shading over the ocean) were calculated using the National Oceanic and Atmospheric Administration (NOAA) Extended Reconstructed SST version 3b dataset³, employed at 2x2° latitude-longitude resolution. The zonal-mean SST is the average SST over the region 50°S-70°S. Sea ice concentration trends (contours over the ocean) were calculated using the Bootstrap sea ice concentration dataset⁴, which has approximately 25x25 km resolution and which was acquired from the National Snow and Ice Data Center (NSIDC). The regional sea-ice extent (SIE) is the sum of all grid points where ice concentration is greater than 15% in each respective region. The regions used are the entire Antarctic domain (shown in Fig. 1 and supplementary Fig. 2), and the Ross-Amundsen, and Amundsen-Bellingshausen regions (as marked in Fig. 1 and Supplementary Fig. 2). Ten-metre wind data (vectors) are from the ERA-Interim reanalysis dataset⁵ employed at 1°x1° latitude-longitude resolution. The Southern Annular Mode (SAM) is defined using the observation-based Marshall SAM index⁶.

Seasonal means for all metrics are defined with respect to the Southern Hemisphere: austral summer (December-February, DJF), austral autumn (March-May, MAM), austral winter (June-August, JJA), and austral spring (September-November, SON). Annual means are calculated over

January–December. All trends are shown as the total linear trend over 1979–2014 (i.e. annual trend multiplied by 36). The statistical significance of trends (hatching for SST and green vectors for wind) follows a Student's two-tailed t-test with threshold of significance set at the 95% confidence level taking into account autocorrelation by using the effective sample size⁷.

Historical and palaeoclimate data analysis.

Figure 2 and Supplementary Figure 3

A full list of data used for this analysis, including references, is given in supplementary Table 1.

We use observations of SAT from Antarctic stations where long historical observations records exist. We use records beginning in 1959 (immediately following the International Geophysical Year) or earlier. These data are sourced from the READER database maintained by the British Antarctic Survey¹. Temperature information from natural archives comes primarily from the published, publicly available database of the PAGES (Past Global Changes) Antarctic2k working group⁸. The ice core water stable isotope records in this database have been assessed as suitable for high-resolution palaeotemperature reconstructions based on their temporal resolution and age control, and cover the last ~300 to 2000 years of climate history. We also use the Gomez⁹ and Ferrigno¹⁰ ice core isotope records to provide detailed climate information for the southwestern Antarctic Peninsula and a moss bank $\delta^{13}\text{C}$ record¹¹ as an additional palaeotemperature indicator from the northern Antarctic Peninsula. Sea ice indicators were derived from a historical record as well as from chemical records preserved within ice cores that are sensitive to sea ice extent¹² and from diatom assemblage data from marine sediment cores¹³. Diatom assemblages from marine sediment cores also provide indicators of past SST changes. Published temperature change reconstructed through inversion of borehole profiles^{14,15} were also compiled. The locations of these borehole temperature profiles are shown in Supplementary Fig. 4. Note that because of temperature diffusion processes in snow and ice, borehole temperature profiles are unable to preserve signals of multi-decadal temperature fluctuations, and resolution is decreasing with time span.

We assess climate signals over four geographic regions (Fig. 2). These regions group together records with similar signals informed by geographic constraints, cross correlation of records and spatial patterns of sea ice trends in the satellite era. The distribution of records was also taken into account when defining reconstruction regions, and in many cases the scarcity of available records necessitates the regions being very broad. The regions we use are: (1) the Antarctic Peninsula including the Bellingshausen Sea and Scotia Sea/northern Weddell Sea including the South Orkney Islands. It is defined by the region south of 55°S and extending to 65°S between 40°W and 60°W, and to 83°S between 60°W and 100°W. (2) The West Antarctic region covers the West Antarctic Ice Sheet, Ross Ice Shelf and the Amundsen and Ross Seas. It is bounded by the latitudes 55°S to 83°S, and the longitudes 100°W to 163°E. (3) The coastal East Antarctic region spans the margin of East Antarctic from the Victoria Land all the way to the Weddell Sea coast, and the adjacent Indian and Atlantic oceans. It is the region south of 55°S and extending to 72°S between 163°E and 80°E, to 74°S between 80°E and 10°W, and to 83°S between 10°W and 60°W (but excluding the region of the northern Weddell Sea assigned to the Antarctic

Peninsula region). (4) The East Antarctic Plateau region approximately follows the 2000m elevation contour and is defined in this study as being south of 83°S between 10°W and 163°E, south of 72°S between 163°E and 80°E, and south of 74°S between 80°E and 10°W. The assignment of the historical and palaeoclimate records to these regions is shown in Supplementary Table 1.

In order to examine regional climate variability and trends over the past 200 years, all records were first binned as 5-year averages. Where records had less than annual resolution (e.g. marine sediment cores, moss bank), they were resampled as pseudo-annuals using a nearest neighbour interpolation method that distributes the measured value across all years that it represents. This ensures that data are attributed with the correct ratio between adjacent 5-year bins. The 5-year binned records were then converted to anomalies (SAT observations and borehole inversions; °C units) or normalised (proxies for SAT, SST and sea ice; σ units) relative to the mean and standard deviation of data in the bins between 1960 and 1990. This normalization step assumes that temperature-proxy variance is the same in all locations within a region, but the validity of this assumption remains to be assessed. With the exception of borehole temperature records, the 5y binned records were then assigned to their respective geographic region and compiled as 5y averages. These regional compilations are presented in Figure 2.

Trend distributions were assessed for proxy records of SAT, SST and SIE using data at annual average or pseudo-annual resolution (Supplementary Fig. 3). To assess the significance of the most recent 36-year trends we calculate the linear trend across the final 36 years of each proxy record. These trends are comparable in length to the satellite-era trends presented in Fig. 1, but are not the same in timing, as the proxy records end at varying times, and none extend to the end of 2014. These are then compared to the distribution of all other earlier 36-year trends in the proxy record to assess the significance with each proxy record of the most recent 36-year trend. This trend assessment is also repeated using 100-year trends for proxy records that cover at least the past 200 years.

CMIP5 model analysis.

Fig. 3, Supplementary Fig. 5

We selected all CMIP5 models that have a minimum of 250 years' duration in their pre-industrial control simulation and at least one Representative Concentration Pathway 8.5 (RCP8.5) simulation (see Supplementary Table 2 for a list of the 38 models included). Prior to computing the trend distributions shown in Fig. 3, we corrected the modelled sea ice extent, SST, SAT and SAM time series for drift. When we found strong nonlinear drift near the start of pre-industrial simulations, we ignored the corresponding portion of the time series for subsequent analysis. We then calculated a linear trend over the full (remaining) length of pre-industrial control experiments and subtracted it from all time series.

From the detrended pre-industrial time series, we computed 36-year linear trends using a 36-year sliding window with a time step of 1 year. The analysed pre-industrial time series totalled a length of around 20000 years (depending on the variable considered, Supplementary Table 2). The distribution of all 36-year trends were compiled by model and then averaged to produce

the distributions in Figure 3 (Fig. 3a-d, blue), a total of more than 15000 overlapping 36-year trends. To gain an estimate of uncertainty in the trend distributions, we applied a Monte Carlo methodology, whereby this process was repeated 1000 times, but with the individual model distributions based on random selections of 10% of all possible 36-year trends. The 5% and 95% levels across the 1000 replicate multi-model distributions produced were used to estimate uncertainty ranges around the pre-industrial 36-year trend distributions (dark blue error bars in Fig. 3a-d). The same process is repeated for Supplementary Figure 5, but using season-specific model data, and without applying the Monte Carlo uncertainty methodology, as we expect seasonal ranges to be very similar to the annual.

Since available historical experiments generally only cover up to year 2005, years 2006-2014 of RCP8.5 simulations were appended to historical 1979-2005 time series to obtain the modelled distributions of 1979-2014 trends (Fig. 3a-d, black/grey). Scenario forcing RCP8.5 was chosen, because it is the best available match to the observed greenhouse gas emissions trajectory over 2006-2014. Between 1 and 12 historical-RCP8.5 simulations per model were available (Supplementary Table 2), giving a total of 90 sample 1979-2014 trends entering the satellite-era trend distributions. Despite the variable length of preindustrial simulations and the variable number of historical-RCP8.5 members across models, we enforced equal model weights in the ensemble distributions of Fig. 3a-d by normalizing each model's contribution by the corresponding number of available 36-year trends. Note also that 500hPa geopotential height fields were not available for the EC-EARTH model, reducing the total number of 36-year SAM index trends included in the control and 1979-2014 ensemble distributions of Fig. 3d to 3210 and 78, respectively.

The same models and experiments were employed for the trend emergence analysis presented in Fig. 3e-h. For each model and each variable, the 5-95% range of control trend distributions is first evaluated for trend lengths increasing from 36 to 122 years, using all possible trends of that length (i.e. stepped by 1 year). Historical-RCP8.5 trends starting in 1979 are then calculated for each trend length (i.e. 36-year trends represent the 1979-2014 interval; 122-year trends represent the 1979-2100 interval) and each model experiment. The historical-RCP8.5 trends are compared to the statistical distribution of trends of the same length in the corresponding model's control simulation, and we compute the proportion of models where the linear trend in the historical-RCP8.5 interval exceeds the 95% distribution of trends in the pre-industrial control (or falls below the 5% distribution in the case of negative sea ice extent trends). To gain an estimate of uncertainty in trend emergence, we again employ a Monte Carlo process, whereby we replicate this test 1000 times, but assess emergence for each model against a random selection of 10% of all possible trends of the same length in the control simulation of the same model. The 5% and 95% range of emergence profiles across the 1000 replicate emergence tests are shown as the orange bars around the black line in Figure 3e-h. As in Fig. 3a-d, we ensure that models have equal weights in the shown cumulative distributions: for a model with n member experiments, each experiment is given a weight of $1/n$ when calculating the cumulative multi-model trend emergence profile.

Supplementary Tables

| Site Name | Record Type | Climate Parameter | Start Year | End Year | Lat. °N | Long. °E | Region | Ref. |
|------------------|-------------------------|-------------------|------------|----------|------------|-------------|-------------------------|---------|
| Amundsen Scott | Observations | SAT | 1957 | 2014 | -90 | 0 | East Antarctic Plateau | 1 |
| Casey | Observations | SAT | 1959 | 2014 | -66.3 | 110.5 | Coastal East Antarctica | 1 |
| Davis | Observations | SAT | 1957 | 2014 | -68.6 | 78 | Coastal East Antarctica | 1 |
| Dumont d'Urville | Observations | SAT | 1956 | 2014 | -66.7 | 140 | Coastal East Antarctica | 1 |
| Esperanza | Observations | SAT | 1945 | 2014 | -63.4 | -57 | Antarctic Peninsula | 1 |
| Faraday | Observations | SAT | 1951 | 2014 | -65.4 | -64.4 | Antarctic Peninsula | 1 |
| Halley | Observations | SAT | 1957 | 2014 | -75.5 | -26.4 | Coastal East Antarctica | 1 |
| Mawson | Observations | SAT | 1954 | 2014 | -67.6 | 62.9 | Coastal East Antarctica | 1 |
| McMurdo | Observations | SAT | 1957 | 2014 | -77.9 | 166.7 | West Antarctica | 1 |
| Mirny | Observations | SAT | 1956 | 2014 | -66.5 | 90.3 | Coastal East Antarctica | 1 |
| Orcadas | Observations | SAT | 1904 | 2014 | -60.7 | -44.7 | Antarctic Peninsula | 1 |
| Syowa | Observations | SAT | 1957 | 2014 | -69 | 39.6 | Coastal East Antarctica | 1 |
| Vostok | Observations | SAT | 1958 | 2014 | -78.5 | 106.9 | East Antarctic Plateau | 1 |
| Byrd | Observations | SAT | 1957 | 2013 | -80 | -119.4 | West Antarctica | 16 |
| Talos Dome | Ice core water isotopes | SAT | 1232 | 1995 | -72.5 | 159.1 | East Antarctic Plateau | 8,17 |
| Law Dome DSS | Ice core water isotopes | SAT | 174 | 2007 | -66.8 | 112.8 | Coastal East Antarctica | 8,18 |
| Plateau Remote | Ice core water isotopes | SAT | 2 | 1986 | -84 | 43 | East Antarctic Plateau | 8,19,20 |

| Site Name | Record Type | Climate Parameter | Start Year | End Year | Lat. °N | Long. °E | Region | Ref. |
|---------------|---------------------------------|-------------------|------------|----------|---------|----------|-------------------------|---------|
| IND-22 B4 | Ice core water isotopes | SAT | 1533 | 1994 | -70.9 | 11.5 | Coastal East Antarctica | 8,21,22 |
| EDML | Ice core water isotopes | SAT | 166 | 1996 | -75 | 0 | East Antarctic Plateau | 23, 8 |
| WAIS 2005A | Ice core water isotopes | SAT | 743 | 2005 | -79.5 | -112.1 | West Antarctica | 24,8 |
| ITASE 00-1 | Ice core water isotopes | SAT | 1674 | 2000 | -79.4 | -111.2 | West Antarctica | 24,8,25 |
| ITASE 00-5 | Ice core water isotopes | SAT | 1719 | 2000 | -77.7 | -124.0 | West Antarctica | 8,24,25 |
| Siple Station | Ice core water isotopes | SAT | 1417 | 1983 | -75.9 | -84.3 | Antarctic Peninsula | 8,25,26 |
| JRI | Ice core water isotopes | SAT | 0 | 2007 | -64.2 | -57.7 | Antarctic Peninsula | 27,28 |
| Gomez | Ice core water isotopes | SAT | 1857 | 2005 | -73.6 | -70.4 | Antarctic Peninsula | 9 |
| Ferrigno | Ice core water isotopes | SAT | 1703 | 2010 | -74.6 | -86.9 | Antarctic Peninsula | 10 |
| Lazarav Bay | Moss bank $\delta^{13}\text{C}$ | SAT | 1863 | 2003 | -69.4 | -71.8 | Antarctic Peninsula | 11 |
| WAIS Divide | Borehole temperature | SAT | 8 | 2007 | -79.5 | -112.1 | West Antarctica | 14 |
| Larissa | Borehole temperature | SAT | 1810 | 2007 | -66 | -64 | Antarctic Peninsula | 29 |
| DML NUS0702 | Borehole temperature | SAT | 1509 | 2008 | -76.1 | 22.5 | East Antarctic Plateau | 30 |
| DML NUS0705 | Borehole temperature | SAT | 1509 | 2008 | -78.7 | 35.6 | East Antarctic Plateau | 30 |
| DML NUS0707 | Borehole temperature | SAT | 1509 | 2008 | -82.1 | 54.9 | East Antarctic Plateau | 30 |
| DML NUS0805 | Borehole temperature | SAT | 1509 | 2009 | -82.6 | 17.9 | East Antarctic Plateau | 30 |
| Mill Island | Borehole temperature | SAT | 1921 | 2011 | -65.6 | 100.8 | Coastal East Antarctica | 31 |

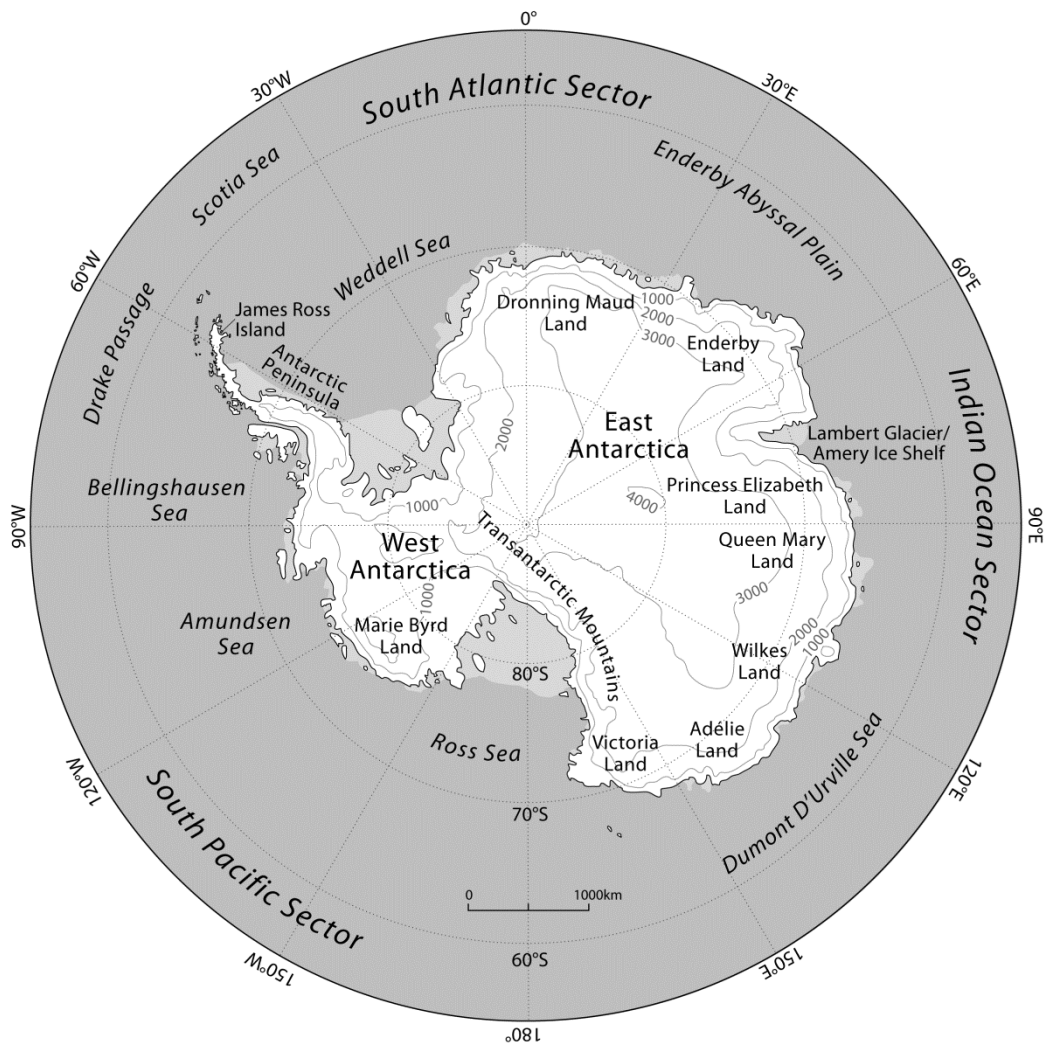
| Site Name | Record Type | Climate Parameter | Start Year | End Year | Lat. °N | Long. °E | Region | Ref. |
|-----------------------|----------------------|-------------------|------------|----------|------------|-------------|-------------------------|------|
| Rutford | Borehole temperature | SAT | 1700 | 2005 | -78.1 | -83.9 | Antarctic Peninsula | 32 |
| MCT18a | Diatom assemblage | SST | 1864 | 1999 | -64.7 | -62.8 | Antarctic Peninsula | 13 |
| MCT38c | Diatom assemblage | SST | 1916 | 2000 | -64.7 | -57.4 | Antarctic Peninsula | 13 |
| CB2010 | Diatom assemblage | SST | 1740 | 2001 | -66.9 | 142.4 | Coastal East Antarctica | 33 |
| West Peninsula stack | Ice core MSA | Winter SIE | 1902 | 1990 | -71.9 | -74.6 | Antarctic Peninsula | 34 |
| Law Dome | Ice core MSA | Winter SIE | 1841 | 1995 | -66.8 | 112.8 | Coastal East Antarctica | 35 |
| South Orkney Fast Ice | Observations | winter SIE | 1903 | 2008 | -60.7 | -44.7 | Antarctic Peninsula | 36 |
| MCT18a | Diatom assemblage | SI duration | 1864 | 1999 | -64.7 | -62.8 | Antarctic Peninsula | 13 |
| MCT38c | Diatom assemblage | SI duration | 1916 | 2000 | -64.7 | -57.4 | Antarctic Peninsula | 13 |
| CB2010 | Diatom assemblage | SI duration | 1740 | 2001 | -66.9 | 142.4 | Coastal East Antarctica | 33 |

Supplementary Table 1: Details of the long observational records and palaeoclimate proxy records used in this study (Fig. 2, Supplementary Fig. 3)

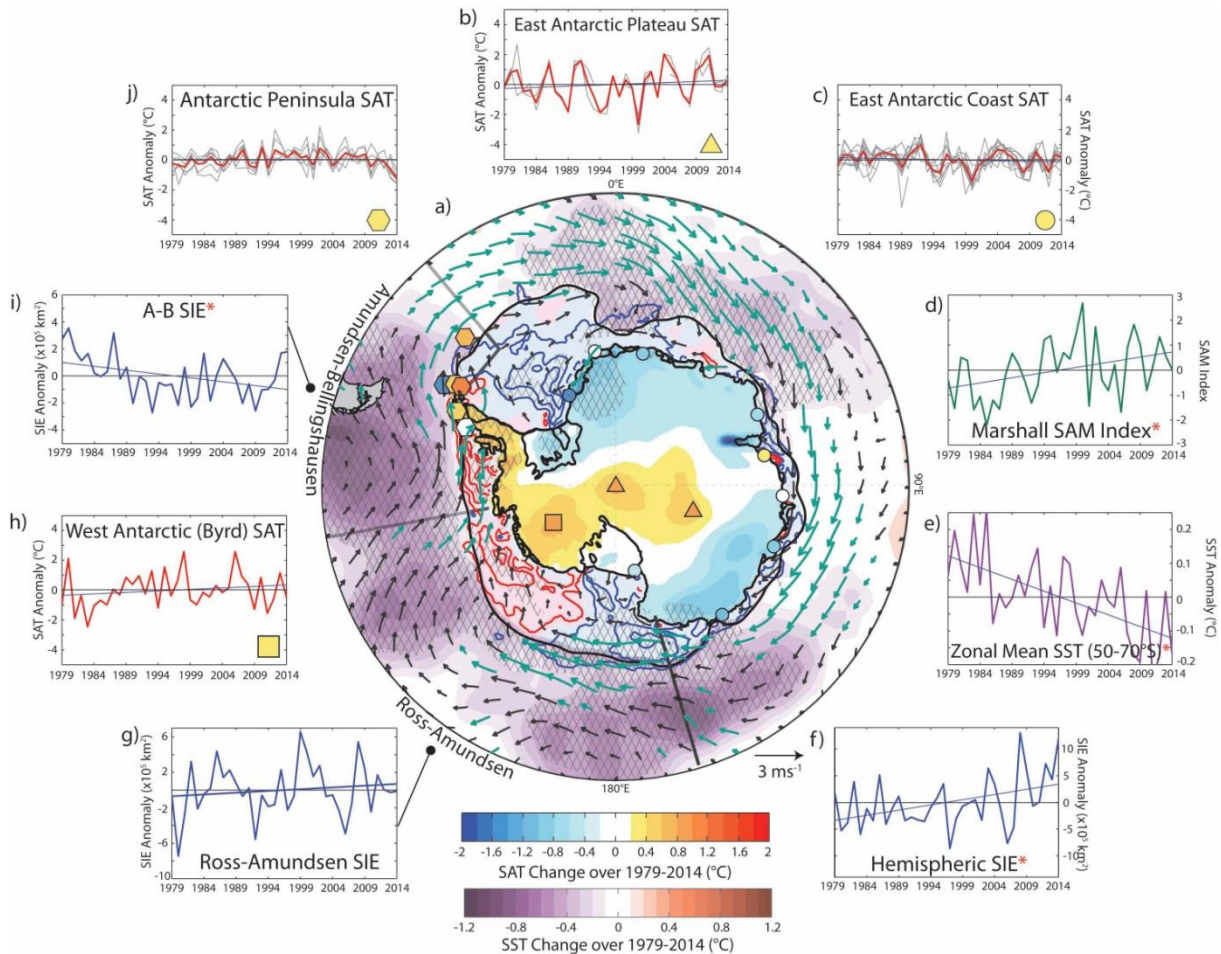
| Model | Analysed pre-industrial control length (years) | Number of historical-RCP8.5 member simulations |
|---------------------------------------|------------------------------------------------|------------------------------------------------|
| ACCESS1.0 | 500 | 1 |
| ACCESS1.3 | 500 | 1 |
| BCC-CSM1.1 | 500 | 1 |
| BCC-CSM1.1m | 400 | 1 |
| BNU-ESM | 550 | 1 |
| CanESM2 | 1096 | 5 |
| CCSM4 | 1051 | 6 |
| CESM1-BGC | 500 | 1 |
| CESM1-CAM5 | 319 | 3 |
| CMCC-CESM | 276 | 1 |
| CMCC-CM | 330 | 1 |
| CMCC-CMS | 500 | 1 |
| CNRM-CM5 | 850 | 5 |
| CSIRO-Mk3.6 | 500 | 10 |
| EC-EARTH | 452 | 12 |
| FGOALS-g2 | 700 | 1 |
| FGOALS-s2 | 501 | 3 |
| FIO-ESM | 800 | 3 |
| GFDL-CM3 | 500 | 1 |
| GFDL-ESM2G | 500 | 1 |
| GFDL-ESM2M | 500 | 1 |
| GISS-E2-H | 540 | 1 |
| GISS-E2-H-CC | 250 | 1 |
| GISS-E2-R | 550 | 2 |
| GISS-E2-R-CC | 250 | 1 |
| HadGEM2-ES | 340 | 4 |
| INM-CM4 | 500 | 1 |
| IPSL-CM5A-LR | 1000 | 4 |
| IPSL-CM5A-MR | 300 | 1 |
| IPSL-CM5B-LR | 300 | 1 |
| MIROC-ESM | 630 | 1 |
| MIROC-ESM-CHEM | 254 | 1 |
| MIROC5 | 700 | 5 |
| MPI-ESM-LR | 1000 | 3 |
| MPI-ESM-MR | 1000 | 1 |
| MRI-CGCM3 | 630 | 1 |
| NorESM1-M | 601 | 1 |
| NorESM1-ME | 252 | 1 |
| Total number of 36-year trends | ~19000 | 90 |

Supplementary Table 2: CMIP5 experiments included in the analysis. The length of pre-industrial control experiments after removal of years characterized by nonlinear drift are indicated for each of the 38 selected models, along with the number of available historical-RCP8.5 members. Note that the SAM index could not be computed for the EC-EARTH model, reducing the total number of 36-year trends entering preindustrial and 1979-2014 ensemble distributions.

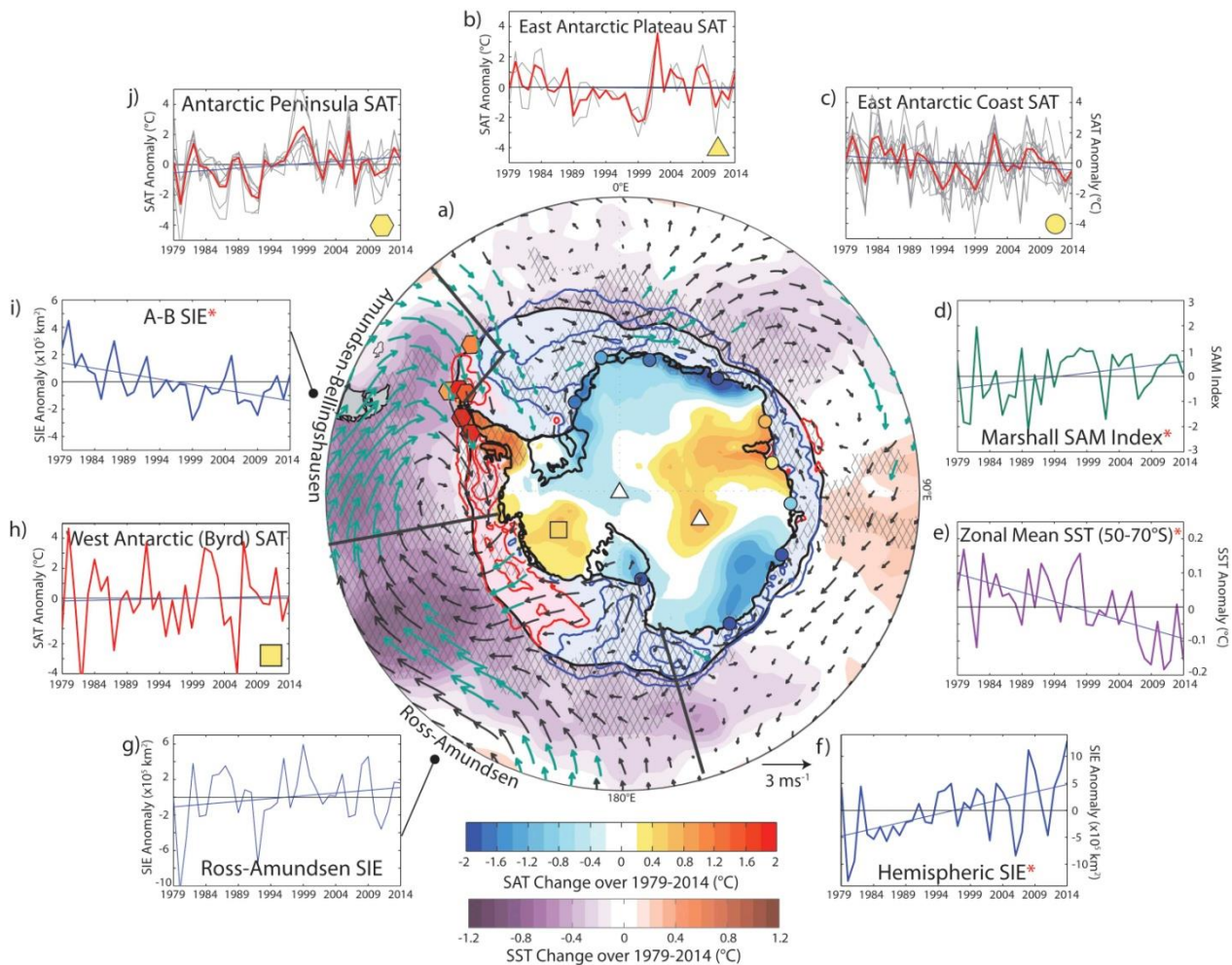
Supplementary Figures



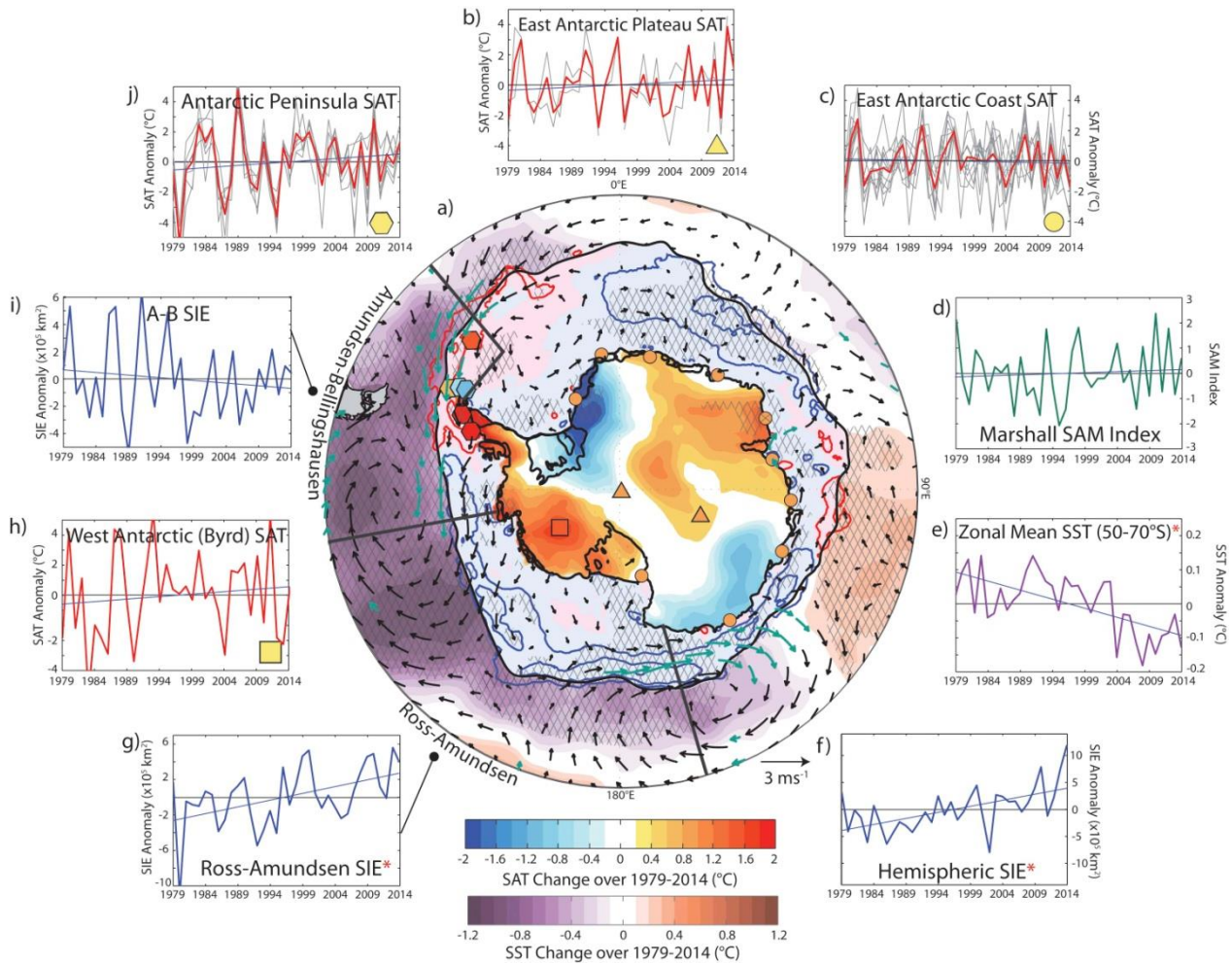
Supplementary Figure 1: Map of the high latitude Southern Hemisphere, including place names mentioned in the text.



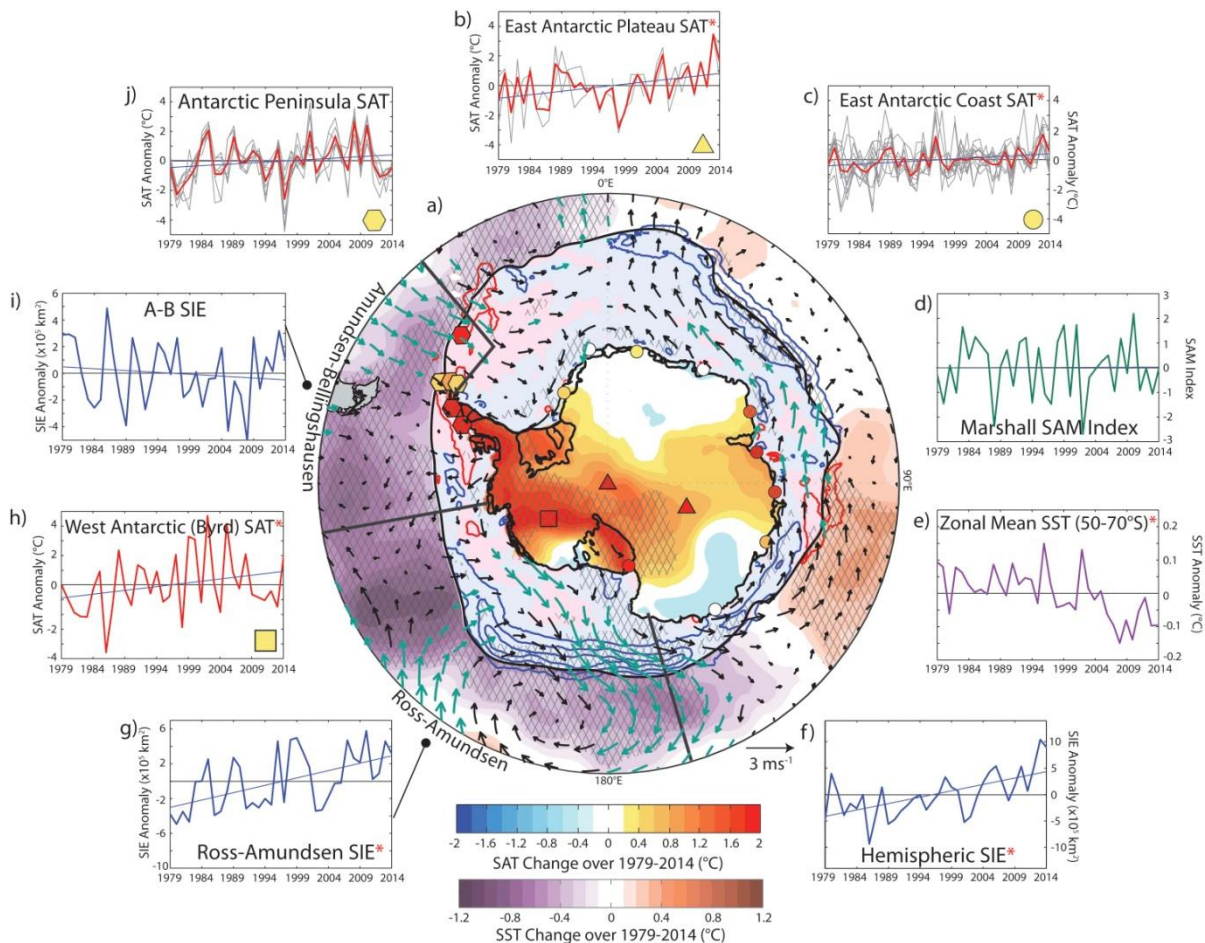
Supplementary Figure 2 a: Antarctic atmosphere-ocean-ice changes over the satellite-observing era for Summer (December, January, February). **a)** Total changes over 1979–2014 in remote sensing annual mean SAT (blue–red shading), station-based SAT (blue–red shaded shapes), sea ice concentration (contours, 10% intervals; red and blue contours, alongside light pink and blue shading beneath, denote negative and positive trends, respectively), SST (purple–red shading), and 10m winds (vectors). Remote sensing SST trends are only shown for areas equatorward of the climatological September SIE (black contour). Hatching and teal vectors highlight trends significant at the 95% level according to two-tailed student t-tests. Note that SAT trends are calculated over 1979–2012 but scaled to represent trends over the 36-year period, 1979–2014. Surrounding figures show time-series of **b)** East Antarctic SAT (circles; red line denotes multi-station mean, grey lines those of individual East Antarctic stations), **c)** the Marshall Southern Annular Mode index (difference in station sea level pressure between 40 and 65°S), **d)** Southern Ocean zonal mean SST (averaged over 50°–70°S), **e)** Southern Hemisphere SIE, **f)** Ross-Amundsen SIE, **g)** West Antarctic SAT (square; Byrd Station), **h)** Amundsen-Bellingshausen SIE, and **i)** Antarctic Peninsula SAT (hexagons; red line denotes multi-station mean, grey lines those of individual Antarctic Peninsula stations). For all time series, blue lines highlight the linear trend, and red asterisks highlight trends that pass a 95% significance two-tailed student t-test. See methods for details on datasets and trend significance calculation.



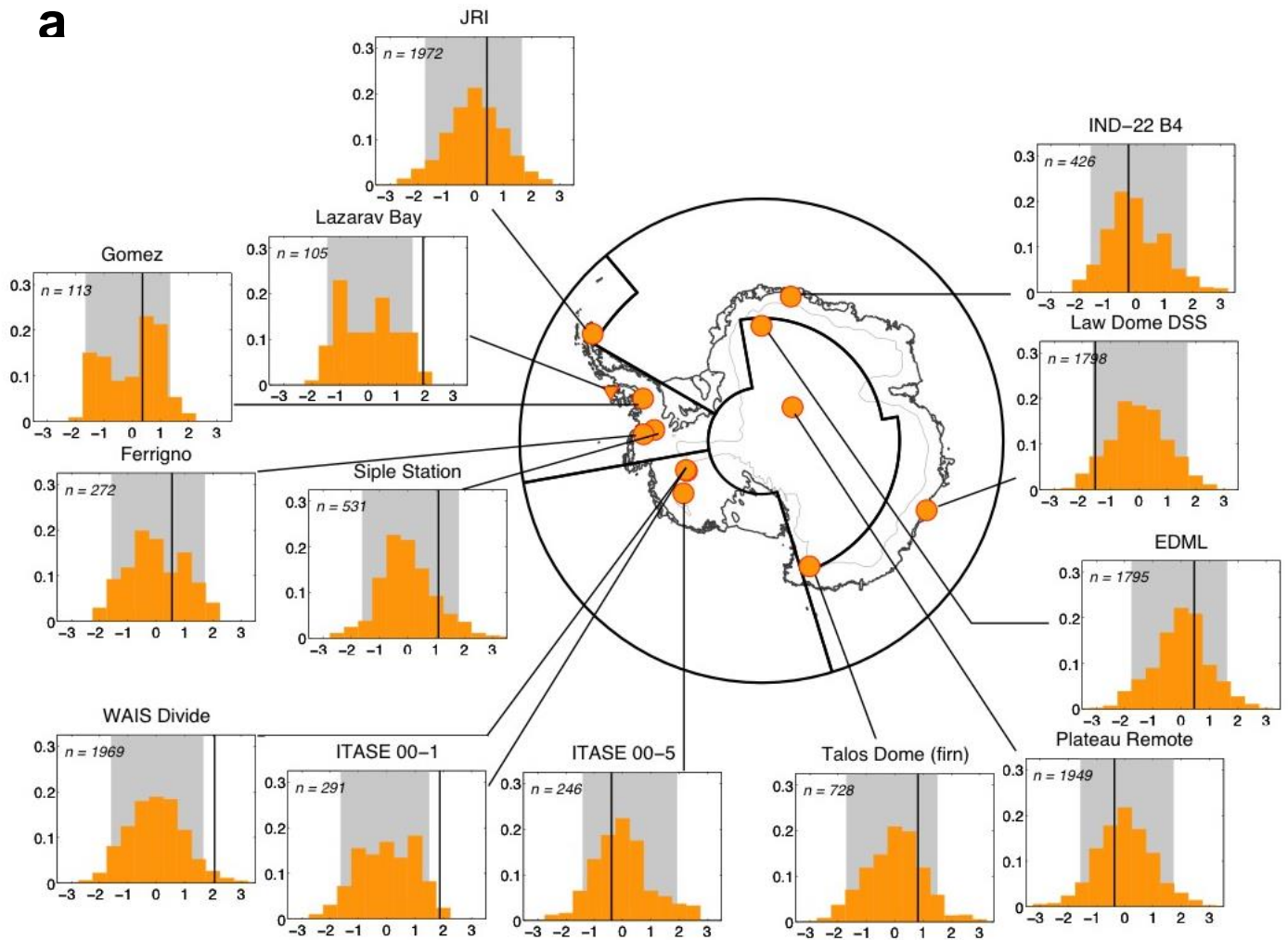
Supplementary Figure 2b: Antarctic atmosphere-ocean-ice changes over the satellite-observing era for Autumn (March, April, May). **a)** Total changes over 1979–2014 in remote sensing annual mean SAT (blue-red shading), station-based SAT (blue-red shaded shapes), sea ice concentration (contours, 10% intervals; red and blue contours, alongside light pink and blue shading beneath, denote negative and positive trends, respectively), sea surface temperature (purple-red shading), and 10m winds (vectors). Remote sensing SST trends are only shown for areas equatorward of the climatological September SIE (black contour). Hatching and teal vectors highlight trends significant at the 95% level according to two-tailed student t-tests. Note that SAT trends are calculated over 1979–2012 but scaled to represent trends over the 36-year period, 1979–2014. Surrounding figures show time-series of **b)** East Antarctic SAT (circles; red line denotes multi-station mean, grey lines those of individual East Antarctic stations), **c)** the Marshall Southern Annular Mode index (difference in station sea level pressure between 40 and 65°S), **d)** Southern Ocean zonal mean SST (averaged over 50°–70°S), **e)** Southern Hemisphere SIE, **f)** Ross-Amundsen SIE, **g)** West Antarctic SAT (square; Byrd Station), **h)** Amundsen-Bellinghshausen SIE, and **i)** Antarctic Peninsula SAT (hexagons; red line denotes multi-station mean, grey lines those of individual Antarctic Peninsula stations). For all time series, blue lines highlight the linear trend, and red asterisks highlight trends that pass a 95% significance two-tailed student t-test. See methods for details on datasets and trend significance calculation.



Supplementary Figure 2c: Antarctic atmosphere-ocean-ice changes over the satellite-observing era for Winter (June, July, August). **a)** Total changes over 1979–2014 in remote sensing annual mean SAT (blue-red shading), station-based SAT (blue-red shaded shapes), sea ice concentration (contours, 10% intervals; red and blue contours, alongside light pink and blue shading beneath, denote negative and positive trends, respectively), sea surface temperature (purple-red shading), and 10m winds (vectors). Remote sensing SST trends are only shown for areas equatorward of the climatological September SIE (black contour). Hatching and teal vectors highlight trends significant at the 95% level according to two-tailed student t-tests. Note that SAT trends are calculated over 1979–2012 but scaled to represent trends over the 36-year period, 1979–2014. Surrounding figures show time-series of **b)** East Antarctic SAT (circles; red line denotes multi-station mean, grey lines those of individual East Antarctic stations), **c)** the Marshall Southern Annular Mode index (difference in station sea level pressure between 40 and 65°S), **d)** Southern Ocean zonal mean SST (averaged over 50°–70°S), **e)** Southern Hemisphere SIE, **f)** Ross-Amundsen SIE, **g)** West Antarctic SAT (square; Byrd Station), **h)** Amundsen-Bellingshausen SIE, and **i)** Antarctic Peninsula SAT (hexagons; red line denotes multi-station mean, grey lines those of individual Antarctic Peninsula stations). For all time series, blue lines highlight the linear trend, and red asterisks highlight trends that pass a 95% significance two-tailed student t-test. See methods for details on datasets and trend significance calculation.

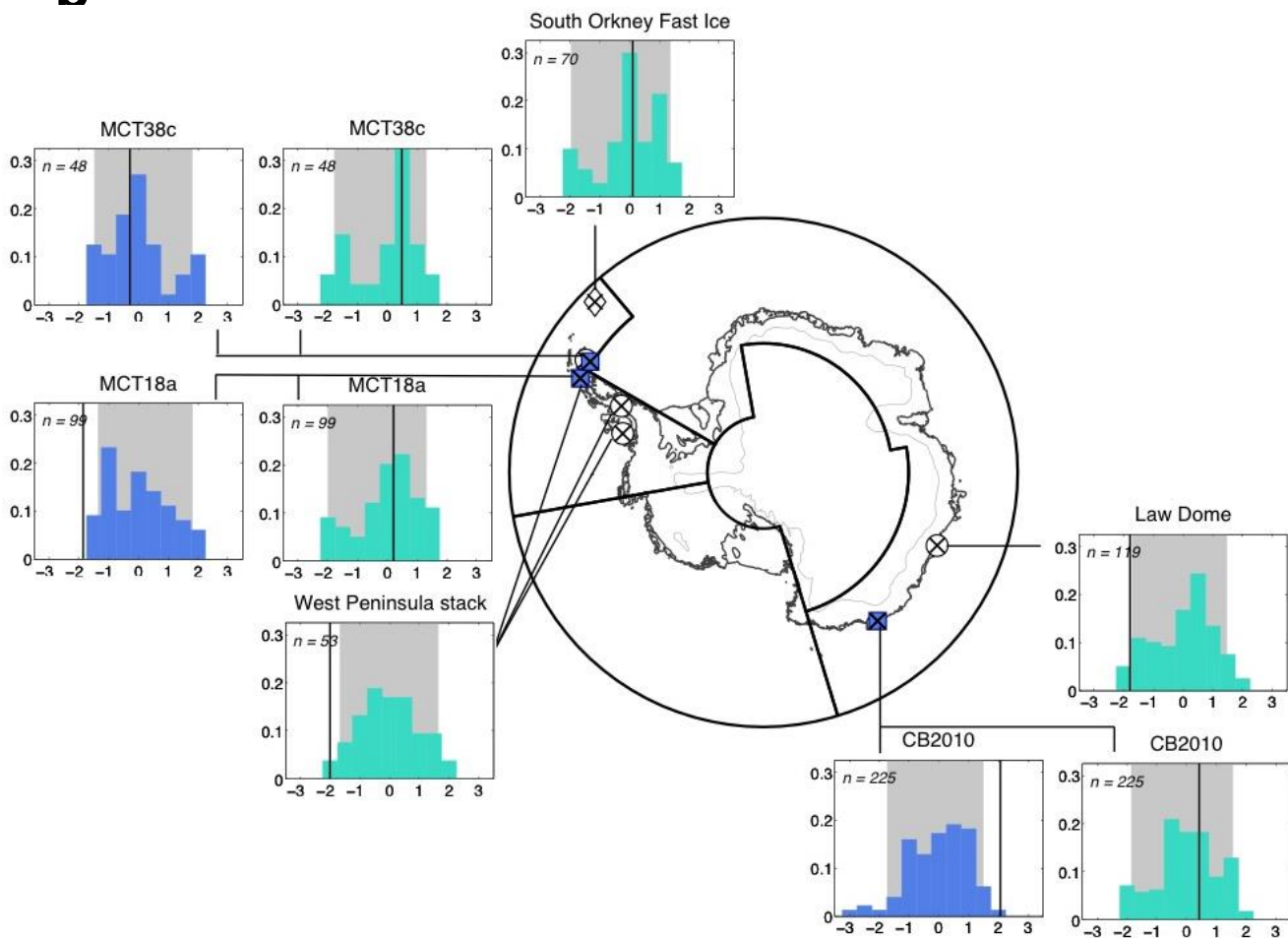


Supplementary Figure 2d: Antarctic atmosphere-ocean-ice changes over the satellite-observing era for Spring (September, October, November). **a)** Total changes over 1979–2014 in remote sensing annual mean SAT (blue–red shading), station-based SAT (blue–red shaded shapes), sea ice concentration (contours, 10% intervals; red and blue contours, alongside light pink and blue shading beneath, denote negative and positive trends, respectively), sea surface temperature (purple–red shading), and 10m winds (vectors). Remote sensing SST trends are only shown for areas equatorward of the climatological September SIE (black contour). Hatching and teal vectors highlight trends significant at the 95% level according to two-tailed student t-tests. Note that SAT trends are calculated over 1979–2012 but scaled to represent trends over the 36-year period, 1979–2014. Surrounding figures show time-series of **b)** East Antarctic SAT (circles; red line denotes multi-station mean, grey lines those of individual East Antarctic stations), **c)** the Marshall Southern Annular Mode index (difference in station sea level pressure between 40 and 65°S), **d)** Southern Ocean zonal mean SST (averaged over 50°–70°S), **e)** Southern Hemisphere SIE, **f)** Ross-Amundsen SIE, **g)** West Antarctic SAT (square; Byrd Station), **h)** Amundsen-Bellingshausen SIE, and **i)** Antarctic Peninsula SAT (hexagons; red line denotes multi-station mean, grey lines those of individual Antarctic Peninsula stations). For all time series, blue lines highlight the linear trend, and red asterisks highlight trends that pass a 95% significance two-tailed student t-test. See methods for details on datasets and trend significance calculation.

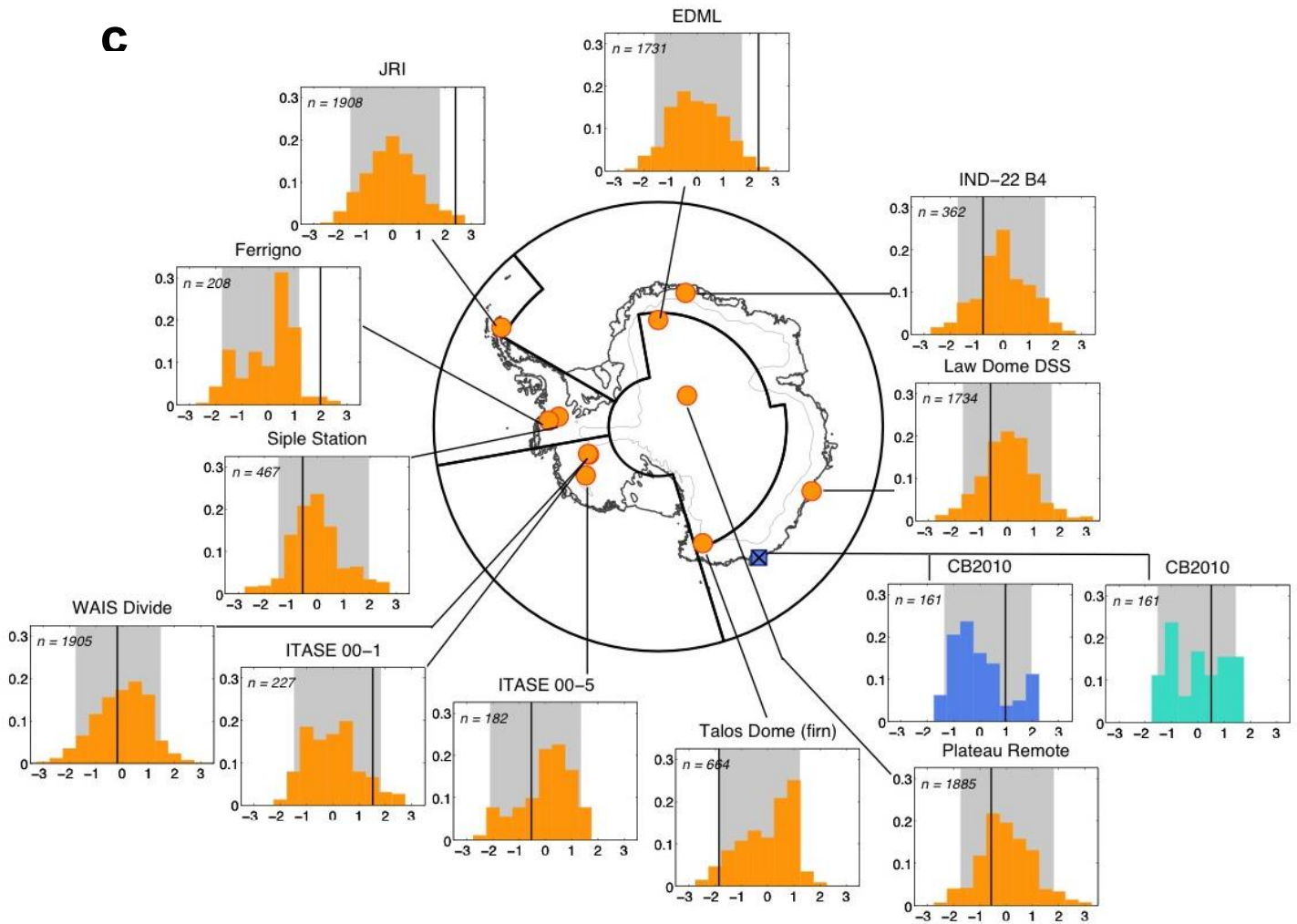


Supplementary Figure 3 (a-c): Significance of recent trends in paleoclimate records. (a) Comparison of the most recent 36y linear trend (black vertical line) in SAT proxy records, compared with all other 36y linear trends in the same SAT proxy record (orange histograms). Grey shading shows the 5-95% range of all 36y trends and n-values denote the total number of 36y trends, excluding the most recent trend. To aid visualisation, the x-axes for all histograms are in normalised trend units (calculated across all trends for a record), and trend occurrence (y-axes) is expressed as a proportion of the total number of trends (n). (b) As in (a) but for SST (blue) and sea ice (cyan) proxy records. (c) As in (a-b) but with trend analysis based on 100y linear trends and shown for SAT (orange), SST (blue) and sea ice (cyan) proxies where records are at least 200 years long.

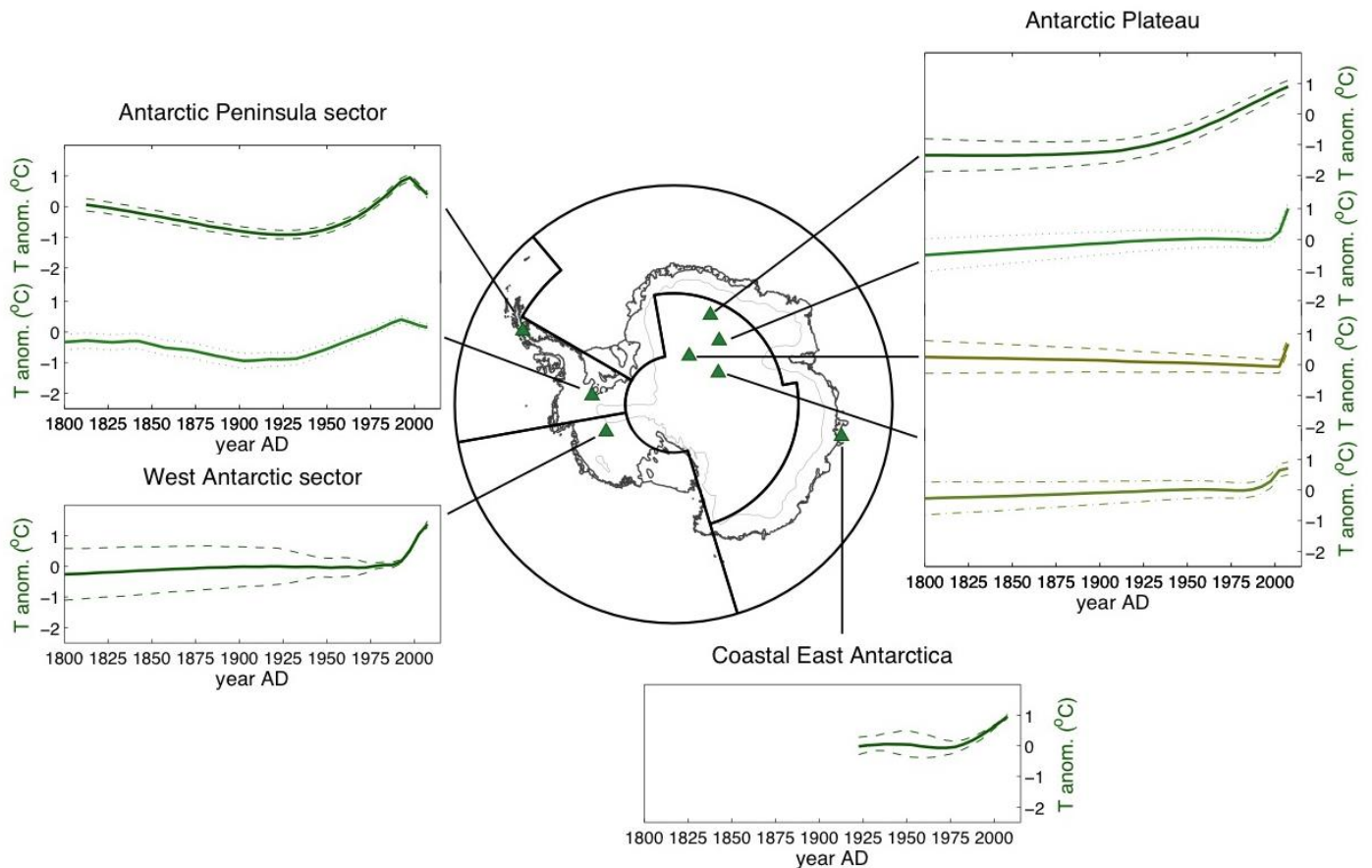
b



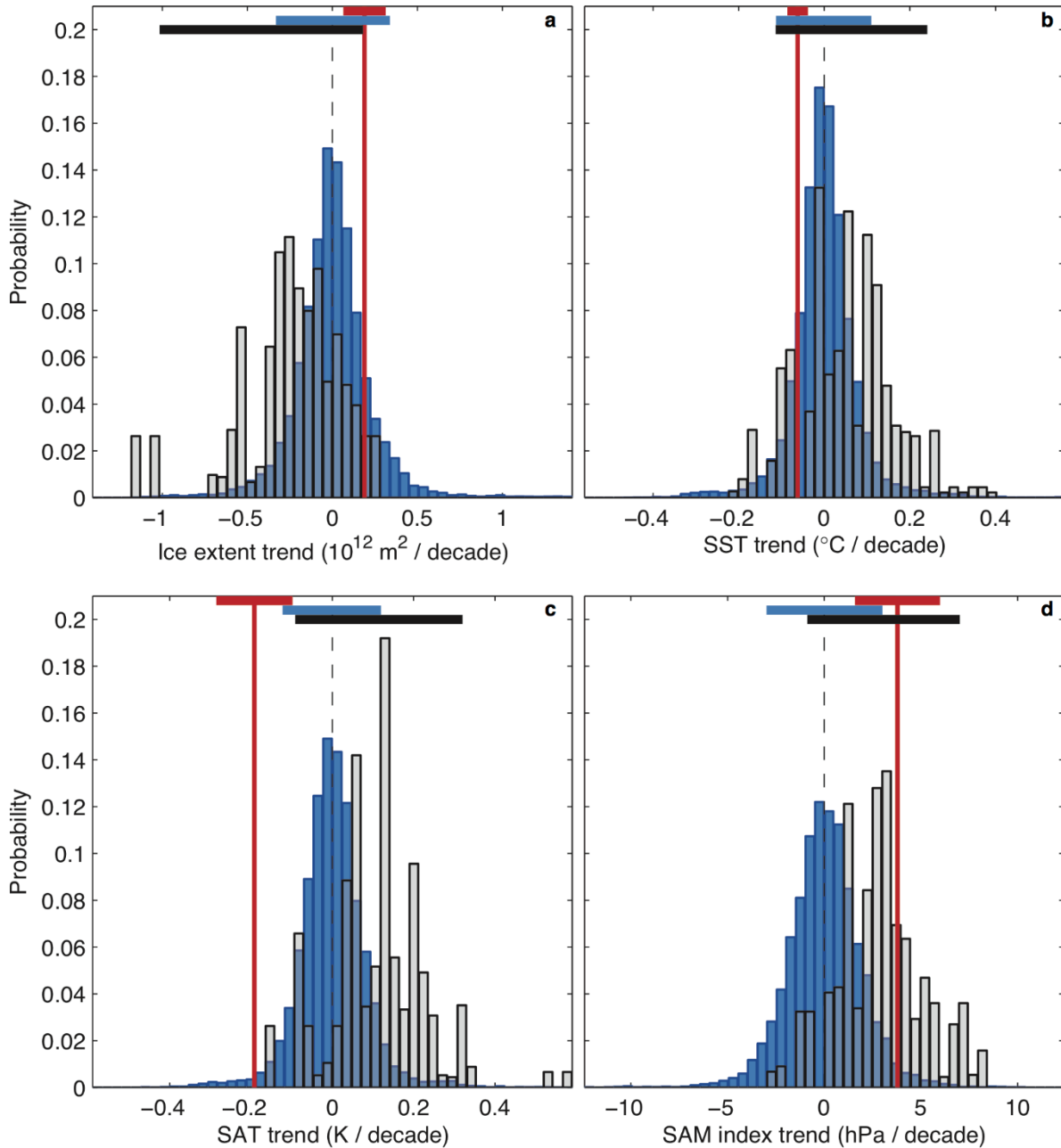
Supplementary Figure 3 (a-c) continued: Significance of recent trends in paleoclimate records. (a) Comparison of the most recent 36y linear trend (black vertical line) in SAT proxy records, compared with all other 36y linear trends in the same SAT proxy record (orange histograms). Grey shading shows the 5-95% range of all 36y trends and n-values denote the total number of 36y trends, excluding the most recent trend. To aid visualisation the x-axes for all histograms are in normalised trend units (calculated across all trends for a record) and trend occurrence (y-axes) is expressed as a proportion of the total number of trends (n). (b) As in (a) but for SST (blue) and sea ice (cyan) proxy records. (c) As in (a-b) but with trend analysis based on 100y linear trends and shown for SAT (orange), SST (blue) and sea ice (cyan) proxies where records are at least 200 years long.



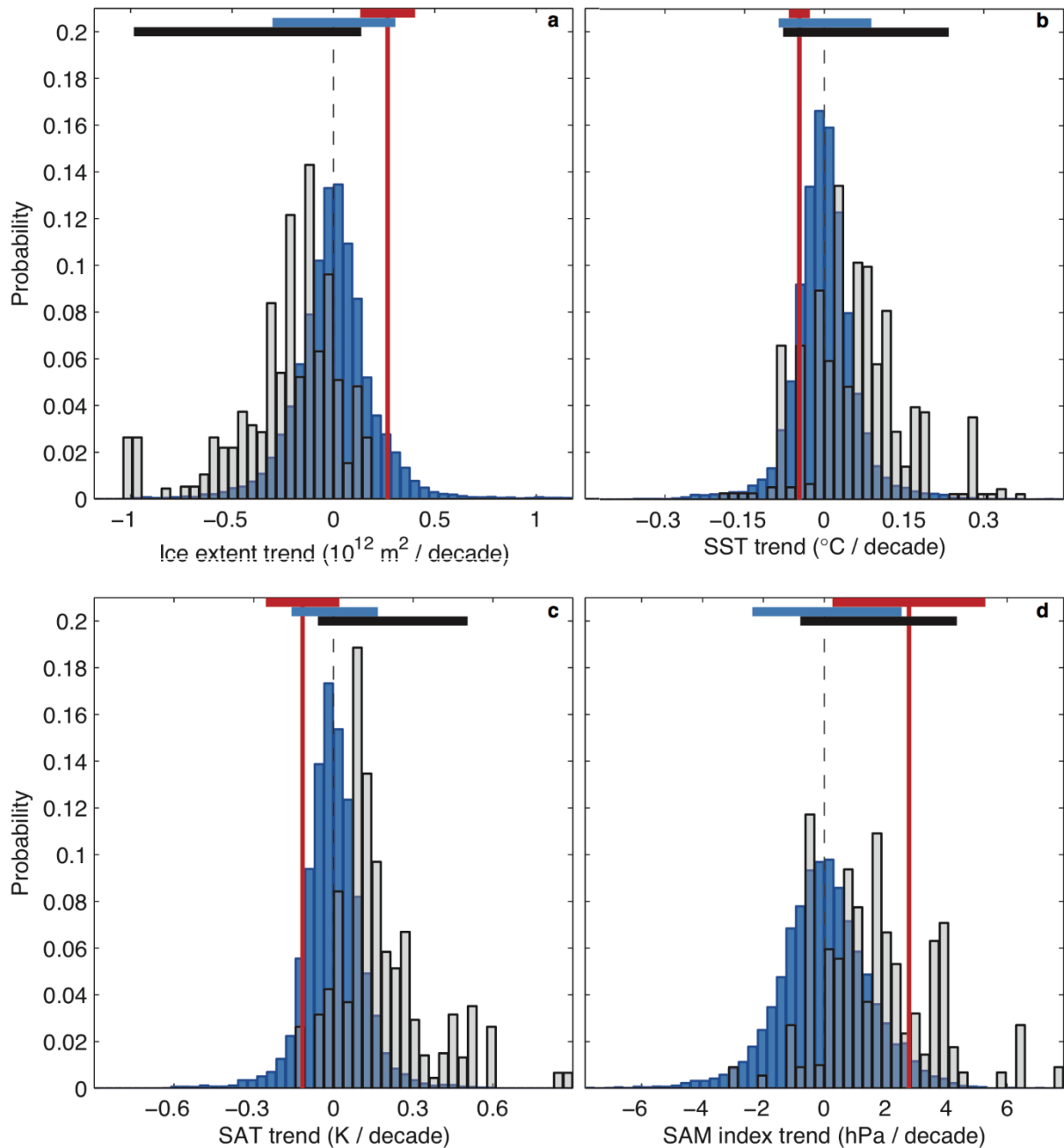
Supplementary Figure 3 (a-c) continued: Significance of recent trends in paleoclimate records. (a) Comparison of the most recent 36y linear trend (black vertical line) in SAT proxy records, compared with all other 36y linear trends in the same SAT proxy record (orange histograms). Grey shading shows the 5-95% range of all 36y trends and n-values denote the total number of 36y trends, excluding the most recent trend. To aid visualisation the x-axes for all histograms are in normalised trend units (calculated across all trends for a record) and trend occurrence (y-axes) is expressed as a proportion of the total number of trends (n). (b) As in (a) but for SST (blue) and sea ice (cyan) proxy records. (c) As in (a-b) but with trend analysis based on 100y linear trends and shown for SAT (orange), SST (blue) and sea ice (cyan) proxies where records are at least 200 years long.



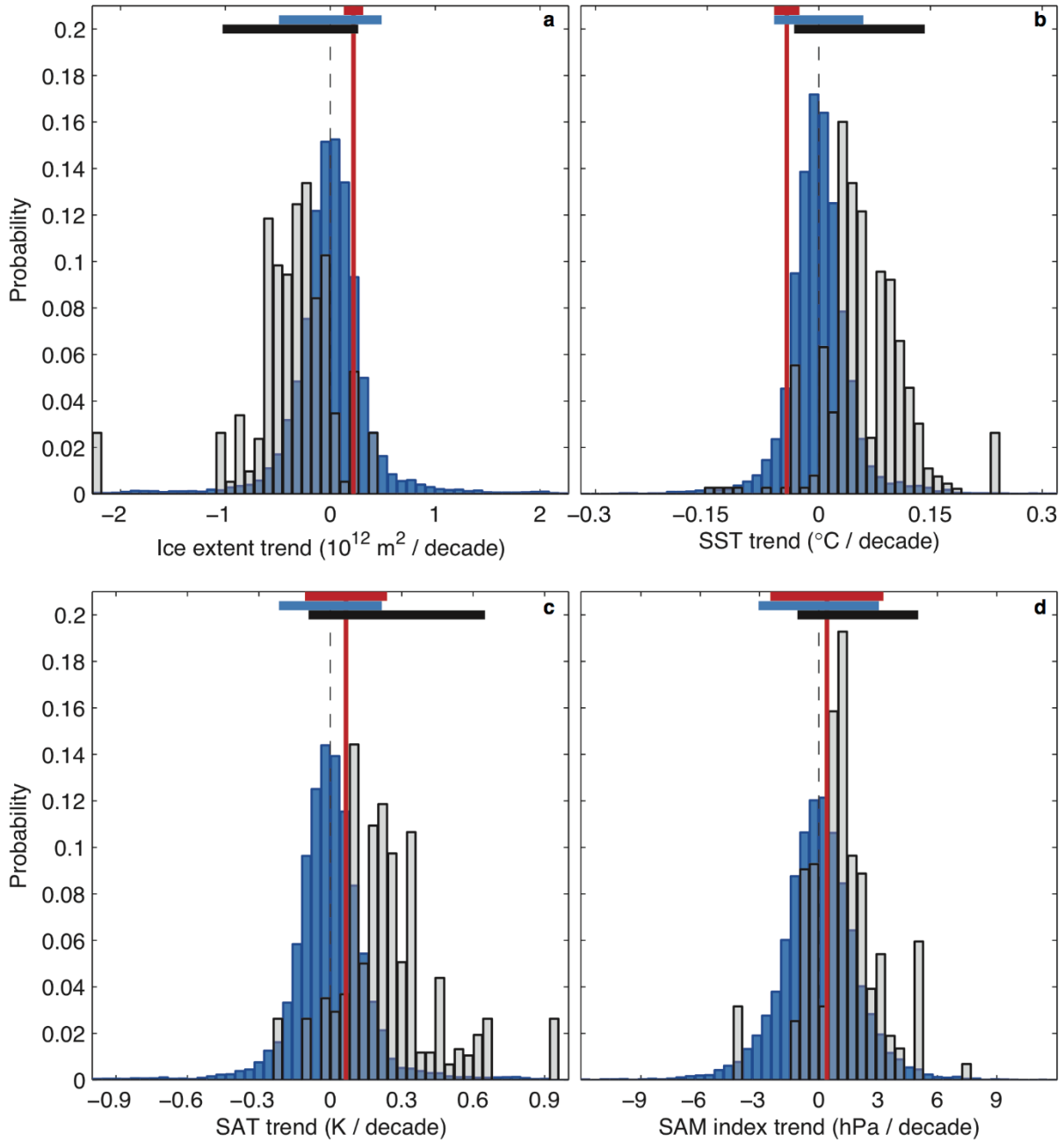
Supplementary Figure 4: Antarctic borehole temperature inversion records. Individual borehole temperature inversions (solid lines) are shown along with their uncertainty bounds (dashed/dotted lines). Colours for each record correspond to those used in Figure 2, but are shown here so that the location of each borehole temperature inversion record can be identified. Details of the individual records provided in Supplementary Table 1.



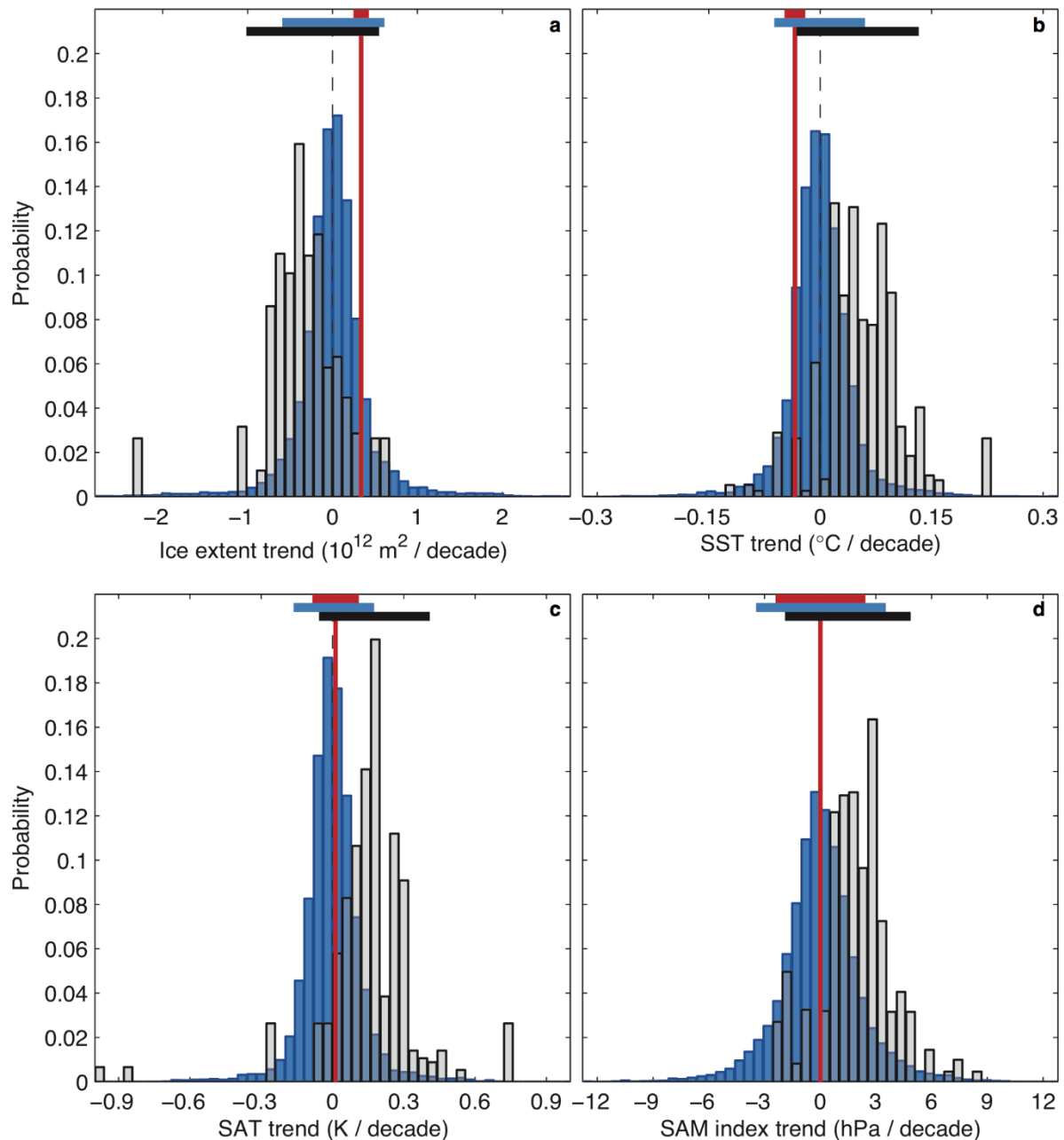
Supplementary Figure 5 DJF: CMIP5 ensemble distributions of 36-year summer (DJF) linear trends in (blue) the ensemble of preindustrial simulations and (black/grey) the ensemble of 1979-2014 historical-RCP8.5 simulations. Panels show **(a)** Southern Hemisphere sea-ice extent, **(b)** mean SST south of 50°S , **(c)** mean SAT south of 50°S and **(d)** SAM index. The red vertical lines correspond to the recent observed 36-year linear trends (1979-2014). Horizontal bars depict (red) the 90% confidence interval of the observed trend, (blue) the 5-95% range of the preindustrial distribution and (black) the 5-95% range of the 1979-2014 trend distribution. Trend calculation methods and data sources are identical to those of Fig. 3a-d.



Supplementary Figure 5 MAM: CMIP5 ensemble distributions of 36-year autumn (MAM) linear trends in (blue) the ensemble of preindustrial simulations and (black/grey) the ensemble of 1979–2014 historical-RCP8.5 simulations. Panels show **(a)** Southern Hemisphere sea-ice extent, **(b)** mean SST south of 50°S , **(c)** mean SAT south of 50°S and **(d)** SAM index. The red vertical lines correspond to the recent observed 36-year linear trends (1979–2014). Horizontal bars depict (red) the 90% confidence interval of the observed trend, (blue) the 5–95% range of the preindustrial distribution and (black) the 5–95% range of the 1979–2014 trend distribution. Trend calculation methods and data sources are identical to those of Fig. 3a–d.



Supplementary Figure 5 JJA: CMIP5 ensemble distributions of 36-year winter (JJA) linear trends in (blue) the ensemble of preindustrial simulations and (black/grey) the ensemble of 1979-2014 historical-RCP8.5 simulations. Panels show **(a)** Southern Hemisphere sea-ice extent, **(b)** mean SST south of 50°S , **(c)** mean SAT south of 50°S and **(d)** SAM index. The red vertical lines correspond to the recent observed 36-year linear trends (1979-2014). Horizontal bars depict (red) the 90% confidence interval of the observed trend, (blue) the 5-95% range of the preindustrial distribution and (black) the 5-95% range of the 1979-2014 trend distribution. Trend calculation methods and data sources are identical to those of Fig. 3a-d.



Supplementary Figure 5 SON: CMIP5 ensemble distributions of 36-year spring (SON) linear trends in (blue) the ensemble of preindustrial simulations and (black/grey) the ensemble of 1979-2014 historical-RCP8.5 simulations. Panels show **(a)** Southern Hemisphere sea-ice extent, **(b)** mean SST south of 50°S , **(c)** mean SAT south of 50°S and **(d)** SAM index. The red vertical lines correspond to the recent observed 36-year linear trends (1979-2014). Horizontal bars depict (red) the 90% confidence interval of the observed trend, (blue) the 5-95% range of the preindustrial distribution and (black) the 5-95% range of the 1979-2014 trend distribution. Trend calculation methods and data sources are identical to those of Fig. 3a-d.

References

- 1 Turner, J. *et al.* The SCAR READER project: Toward a high-quality database of mean Antarctic meteorological observations. *Journal of Climate* **17**, 2890-2898, doi:10.1175/1520-0442(2004).
- 2 Nicolas, J. P. & Bromwich, D. H. New Reconstruction of Antarctic Near-Surface Temperatures: Multidecadal Trends and Reliability of Global Reanalyses. *Journal of Climate* **27**, 8070-8093, doi:10.1175/jcli-d-13-00733.1 (2014).
- 3 Smith, T. M., Reynolds, R. W., Peterson, T. C. & Lawrimore, J. Improvements to NOAA's historical merged land-ocean surface temperature analysis (1880-2006). *Journal of Climate* **21**, 2283-2296, doi:10.1175/2007jcli2100.1 (2008).
- 4 Comiso, J. C. Bootstrap Sea Ice Concentrations from Nimbus-7 SMMR and DMSP SSM/I-SSMIS, Version 2 [NSIDC-0-79]. National Snow and Ice Data Center Distributed Active, Boulder, Colorado, doi: <http://dx.doi.org/10.5067/J6JQLS9EJ5HU>. (2000, 2015 update).
- 5 Dee, D. P. *et al.* The ERA-Interim reanalysis: configuration and performance of the data assimilation system. *Quarterly Journal of the Royal Meteorological Society* **137**, 553-597, doi:10.1002/qj.828 (2011).
- 6 Marshall, G. J. Trends in the southern annular mode from observations and reanalyses. *Journal of Climate* **16**, 4134-4143, doi:10.1175/1520-0442 (2003).
- 7 Santer, B. D. *et al.* Statistical significance of trends and trend differences in layer-average atmospheric temperature time series. *Journal of Geophysical Research-Atmospheres* **105**, 7337-7356, doi:10.1029/1999jd901105 (2000).
- 8 PAGES 2K Consortium. Continental-scale temperature variability during the past two millennia. *Nature Geoscience* **6**, 339-346, doi:10.1038/ngeo1797 (2013).
- 9 Thomas, E. R., Marshall, G. J. & McConnell, J. R. A doubling in snow accumulation in the western Antarctic Peninsula since 1850. *Geophysical Research Letters* **35**, doi:10.1029/2007gl032529 (2008).
- 10 Thomas, E. R., Bracegirdle, T. J., Turner, J. & Wolff, E. W. A 308 year record of climate variability in West Antarctica. *Geophysical Research Letters* **40**, 5492-5496, doi:10.1002/2013gl057782 (2013).
- 11 Royles, J. *et al.* Plants and Soil Microbes Respond to Recent Warming on the Antarctic Peninsula. *Current Biology* **23**, 1702-1706, doi:10.1016/j.cub.2013.07.011 (2013).
- 12 Abram, N. J., Wolff, E. W. & Curran, M. A. J. A review of sea ice proxy information from polar ice cores. *Quaternary Science Reviews* **79**, 168-183, doi:10.1016/j.quascirev.2013.01.011 (2013).
- 13 Barbara, L., Crosta, X., Schmidt, S. & Masse, G. Diatoms and biomarkers evidence for major changes in sea ice conditions prior the instrumental period in Antarctic Peninsula. *Quaternary Science Reviews* **79**, 99-110, doi:10.1016/j.quascirev.2013.07.021 (2013).
- 14 Orsi, A. J., Cornuelle, B. D. & Severinghaus, J. P. Little Ice Age cold interval in West Antarctica: Evidence from borehole temperature at the West Antarctic Ice Sheet (WAIS) Divide. *Geophysical Research Letters* **39**, doi:10.1029/2012gl051260 (2012).

- 15 Clow, G. D. The extent of temporal smearing in surface-temperature histories derived from borehole temperature measurements. *Palaeogeography Palaeoclimatology Palaeoecology* **98**, 81-86, doi:10.1016/0031-0182(92)90189-c (1992).
- 16 Bromwich, D. H. *et al.* Central West Antarctica among the most rapidly warming regions on Earth. *Nature Geoscience* **6**, 139-145, doi:10.1038/ngeo1671 (2013).
- 17 Stenni, B. *et al.* Eight centuries of volcanic signal and climate change at Talos Dome (East Antarctica). *Journal of Geophysical Research-Atmospheres* **107**, doi:10.1029/2000jd000317 (2002).
- 18 Plummer, C. T. *et al.* An independently dated 2000-yr volcanic record from Law Dome, East Antarctica, including a new perspective on the dating of the 1450s CE eruption of Kuwae, Vanuatu. *Climate of the Past* **8**, 1929-1940, doi:10.5194/cp-8-1929-2012 (2012).
- 19 Cole-Dai, J. H., Mosley-Thompson, E., Wight, S. P. & Thompson, L. G. A 4100-year record of explosive volcanism from an East Antarctica ice core. *Journal of Geophysical Research-Atmospheres* **105**, 24431-24441, doi:10.1029/2000jd900254 (2000).
- 20 Mosley-Thompson, E. Holocene Climate Changes Recoded in an East Antarctica Ice Core, in *Climatic Variations and Forcing Mechanisms of the Last 2000 years* (eds P. D Jones, R. S. Bradley, & J. Jouzel) 263-269 (Springer-Verlag, 1996).
- 21 Thamban, M. *et al.* Aerosol perturbations related to volcanic eruptions during the past few centuries as recorded in an ice core from the Central Dronning Maud Land, Antarctica. *Current Science* **91**, 1200-1207 (2006).
- 22 Laluraj, C. M. *et al.* Nitrate records of a shallow ice core from East Antarctica: Atmospheric processes, preservation and climatic implications. *Holocene* **21**, 351-356, doi:10.1177/0959683610374886 (2011).
- 23 Graf, W. *et al.* Stable-isotope records from Dronning Maud Land, Antarctica. Supplement to *Annals of Glaciology*, 35, 195-201, doi:10.1594/PANGAEA.104862 (2002).
- 24 Steig, E. J. *et al.* Recent climate and ice-sheet changes in West Antarctica compared with the past 2,000 years. *Nature Geoscience* **6**, 372-375, doi:10.1038/ngeo1778 (2013).
- 25 Schneider, D. P. *et al.* Antarctic temperatures over the past two centuries from ice cores. *Geophysical Research Letters* **33**, doi:10.1029/2006gl027057 (2006).
- 26 Mosley-Thompson, E., Thompson, L. G., Grootes, P. M., & Gundestrup, N. Little Ice Age (neoglacial) palaeoenvironmental conditions at Siple Station. *Annals of Glaciology* **14**, 199-204 (1990).
- 27 Mulvaney, R. *et al.* Recent Antarctic Peninsula warming relative to Holocene climate and ice-shelf history. *Nature* **489**, 141-144, doi:10.1038/nature11391 (2012).
- 28 Abram, N. J. *et al.* Acceleration of snow melt in an Antarctic Peninsula ice core during the twentieth century. *Nature Geoscience* **6**, 404-411, doi:10.1038/ngeo1787 (2013).
- 29 Zagorodnov, V. *et al.* Borehole temperatures reveal details of 20th century warming at Bruce Plateau, Antarctic Peninsula. *Cryosphere* **6**, 675-686, doi:10.5194/tc-6-675-2012 (2012).
- 30 Muto, A., Scambos, T. A., Steffen, K., Slater, A. G. & Clow, G. D. Recent surface temperature trends in the interior of East Antarctica from borehole firn temperature measurements and geophysical inverse methods. *Geophysical Research Letters* **38**, doi:10.1029/2011gl048086 (2011).

- 31 Roberts, J. L. *et al.* Borehole temperatures reveal a changed energy budget at Mill Island, East Antarctica, over recent decades. *Cryosphere* **7**, 263-273, doi:10.5194/tc-7-263-2013 (2013).
- 32 Barrett, B. E., Nicholls, K. W., Murray, T., Smith, A. M. & Vaughan, D. G. Rapid recent warming on Rutford Ice Stream, West Antarctica, from borehole thermometry. *Geophysical Research Letters* **36**, doi:10.1029/2008gl036369 (2009).
- 33 Campagne, P. *et al.* Glacial ice and atmospheric forcing on the Mertz Glacier Polynya over the past 250 years. *Nature Communications* **6**, doi:10.1038/ncomms7642 (2015).
- 34 Abram, N. J. *et al.* Ice core evidence for a 20th century decline of sea ice in the Bellingshausen Sea, Antarctica. *Journal of Geophysical Research-Atmospheres* **115**, doi:10.1029/2010jd014644 (2010).
- 35 Curran, M. A. J., van Ommen, T. D., Morgan, V. I., Phillips, K. L. & Palmer, A. S. Ice core evidence for Antarctic sea ice decline since the 1950s. *Science* **302**, 1203-1206, doi:10.1126/science.1087888 (2003).
- 36 Murphy, E. J., Clarke, A., Abram, N. J. & Turner, J. Variability of sea-ice in the northern Weddell Sea during the 20th century. *Journal of Geophysical Research-Oceans* **119**, 4549-4572, doi:10.1002/2013jc009511 (2014).